Cell Reports

Article

RTEL1 helicase counteracts RAD51-mediated homologous recombination and fork reversal to safeguard replicating genomes

Graphical abstract

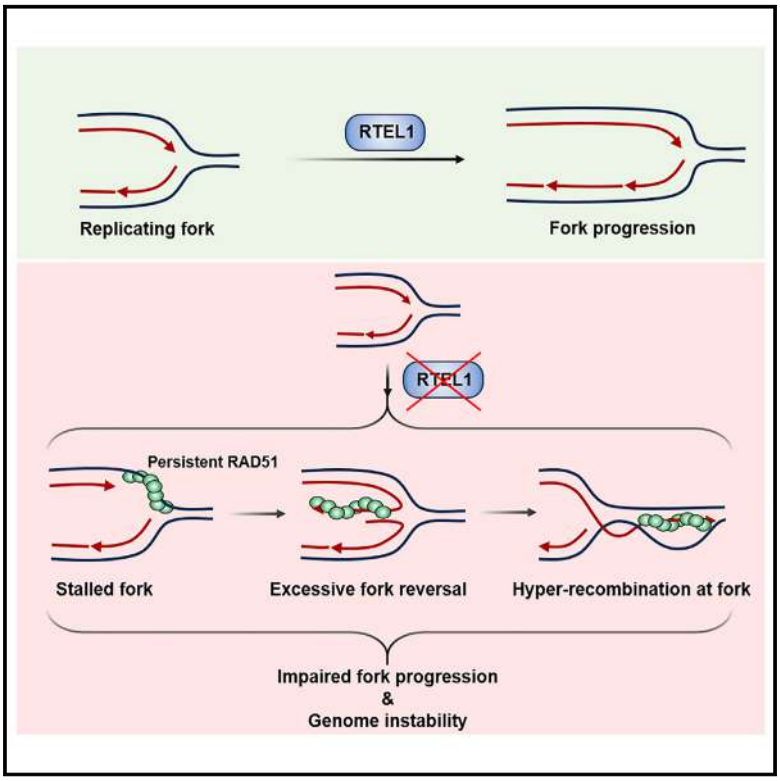

Highlights

- RTEL1 suppresses hyper-recombination during DNA replication
- RTEL1 controls RAD51-mediated fork reversal
- RTEL1 prevents excessive accumulation of RAD51 and RAD51 paralogs at the stalled fork sites
- RTEL1 helicase function is critical for suppressing hyper-recombination

Authors

Suruchi Dixit, Tarun Nagraj, Debanjali Bhattacharya, ..., Rajani Kant Chittela, Kumar Somyajit, Ganesh Nagaraju

Correspondence

ksom@sdu.dk (K.S.), nganesh@iisc.ac.in (G.N.)

In brief

The role of RTEL1 helicase during replication is less understood. Here, Dixit et al. identify the role of RTEL1 in restricting inappropriate recombination events during replication. RTEL1 prevents RAD51 accumulation at stalled fork sites and suppresses excessive RAD51-mediated fork reversal to facilitate genome duplication.

Dixit et al., 2024, Cell Reports *43*, 114594
August 27, 2024
https://doi.org/10.1016/j.celrep.2024.114594

CellPress

Cell Reports

CellPress
OPEN ACCESS

Article

RTEL1 helicase counteracts RAD51-mediated homologous recombination and fork reversal to safeguard replicating genomes

Suruchi Dixit,[1] Tarun Nagraj,[1,4] Debanjali Bhattacharya,[1,4] Sneha Saxena,[1] Satyaranjan Sahoo,[1] Rajani Kant Chittela,[2] Kumar Somyajit,[1,3,*] and Ganesh Nagaraju[1,5,*]

[1]Department of Biochemistry Indian Institute of Science, Bangalore 560012, India
[2]Applied Genomics Section, Bioscience Group, Bhabha Atomic Research Centre, Mumbai 400085, India
[3]Functional Genomics & Metabolism Research Unit, Department of Biochemistry and Molecular Biology, University of Southern Denmark, Campusvej 55, Odense M 5230, Denmark
[4]These authors contributed equally
[5]Lead contact
*Correspondence: ksom@sdu.dk (K.S.), nganesh@iisc.ac.in (G.N.)
https://doi.org/10.1016/j.celrep.2024.114594

SUMMARY

Homologous recombination (HR) plays an essential role in the repair of DNA double-strand breaks (DSBs), replication stress responses, and genome maintenance. However, unregulated HR during replication can impair genome duplication and compromise genome stability. The mechanisms underlying HR regulation during DNA replication are obscure. Here, we find that RTEL1 helicase, RAD51, and RAD51 paralogs are enriched at stalled replication sites. The absence of RTEL1 leads to an increase in the RAD51-mediated HR and fork reversal during replication and affects genome-wide replication, which can be rescued by co-depleting RAD51 and RAD51 paralogs. Interestingly, co-depletion of fork remodelers such as SMARCAL1/ZRANB3/HLTF/FBH1 and expression of HR-defective RAD51 mutants also rescues replication defects in RTEL1-deficient cells. The anti-recombinase function of RTEL1 during replication depends on its interaction with PCNA and helicase activity. Together, our data identify the role of RTEL1 helicase in restricting RAD51-mediated fork reversal and HR activity to facilitate error-free genome duplication.

INTRODUCTION

Accurate transmission of genetic information during every round of cell division is crucial for maintaining genomic integrity. However, DNA replication is challenged by obstacles arising from both endogenous and exogenous sources. The replication fork slows or stalls when it encounters lesions on the template DNA, nucleotide depletion, DNA secondary structures, and topological constraints.[1,2] Defects in stabilizing or restarting the stalled forks can lead to chromosomal instability and cancer-susceptible genetic diseases. Cells have evolved with multiple mechanisms to deal with replication problems, thereby protecting the genome from accumulations of mutations, diseases, and cancer.[2,3] Stalled forks undergo remodeling by various DNA translocases/helicases including BLM, WRN, and FANCM and SNF2 family translocases SMARCAL1, ZRANB3, and HLTF.[4–6] The reversed forks slow down DNA replication and stabilize and facilitate the restart of stalled forks.[6–8] Nonetheless, reversed forks are also susceptible to degradation by nucleases such as MRE11, EXO1, and DNA2, thereby leading to fork breakage and genome instability.[5,9]

Homologous recombination (HR) is a fundamental cellular process conserved across all domains of life and plays an essential role in the repair of DNA double-strand breaks (DSBs), genome maintenance, and tumor suppression.[10–13] BRCA1, BRCA2, RAD51, and RAD51 paralogs are crucial for repairing DSBs by HR and maintaining genome integrity.[10,14–19] Germline mutations in these genes are known to cause Fanconi anemia and breast and ovarian cancers.[18,20] In addition to their canonical role in DSB repair, these proteins have evolved with repair-independent functions in protecting the stalled DNA replication forks from nucleolytic degradation.[5,9,21–23] RAD51 and RAD51 paralogs also participate in the restart of stalled/collapsed replication forks.[24–26] Although HR is critical for DNA repair and replication stress responses, unregulated HR can lead to the accumulation of mutations and various types of genome rearrangements.[27–31] However, the factors and molecular mechanisms that regulate HR during genome duplication are less clear.

RTEL1 is a 5'→3' DNA helicase/translocase that belongs to the SF2 and Fe-S cluster family of helicases.[32] Germline mutations in *RTEL1* cause Hoyeraal-Hreidarsson syndrome and dyskeratosis congenita, characterized by developmental abnormalities, bone marrow failure, and telomere dysfunction.[32–34] Individuals with mutations in *RTEL1* are also predisposed to high-grade gliomas, astrocytomas, and glioblastomas.[33] RTEL1 plays an important role in telomere homeostasis by participating in

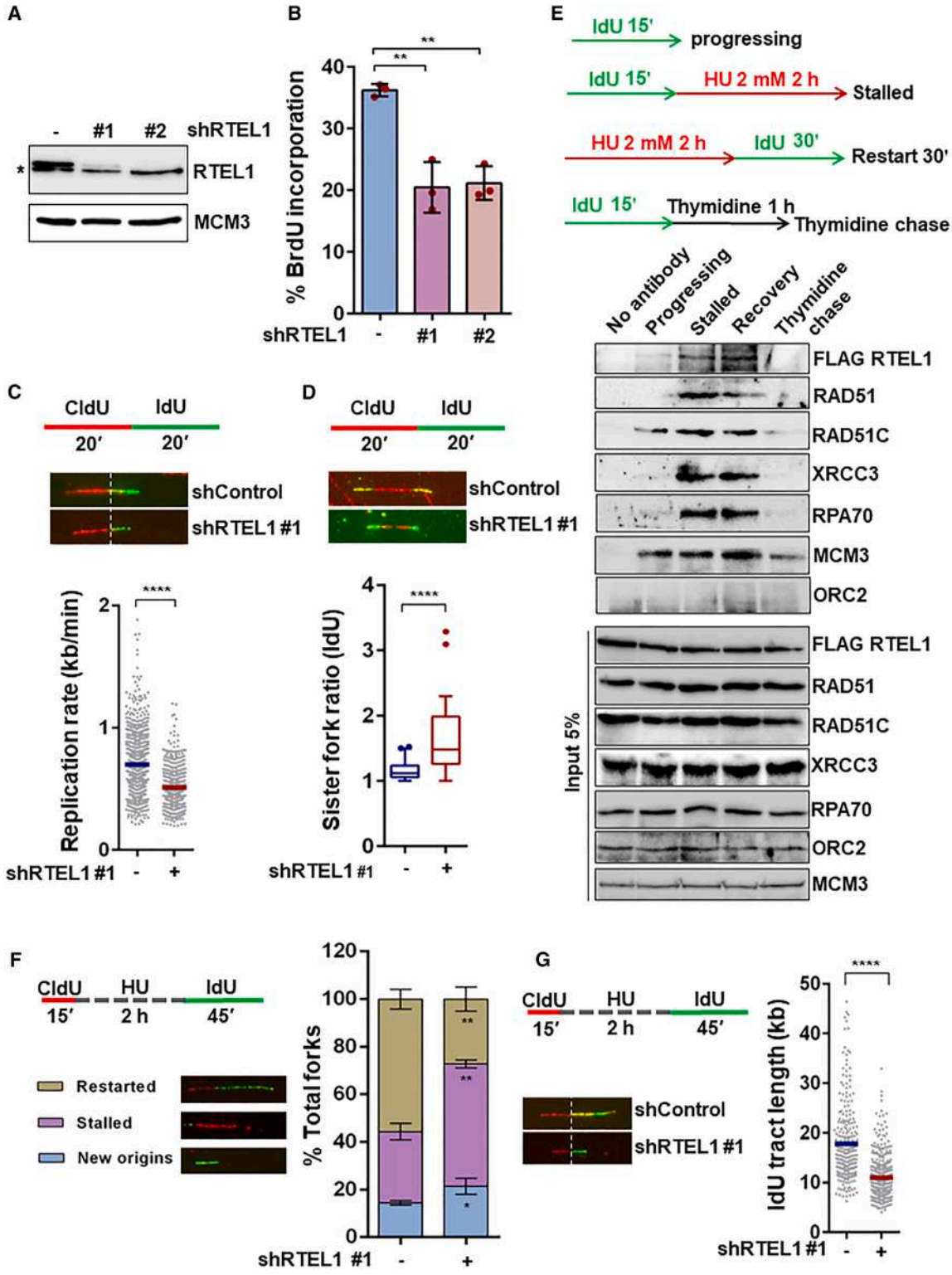

Figure 1. RTEL1 localizes to stalled forks and facilitates genome-wide replication in human cells

(A) A representative western blot showing depletion of RTEL1 in U2OS cells. #1 (UTR specific) and #2 (gene specific) represent two independent shRNAs. (*) indicates a nonspecific band. MCM3 serves as a loading control.

(B) The bar graph shows the quantification of percentage of BrdU incorporation in control and RTEL1-depleted cells from 3 independent experiments. Data are represented as mean ± SD. One-way ANOVA test, *$p < 0.05$, **$p < 0.01$, ***$p < 0.001$, and ****$p < 0.0001$. n.s., nonsignificant.

(legend continued on next page)

T-loop resolution, G4 DNA, and R-loop resolution.[35–37] *C. elegans* and human cells lacking RTEL1 exhibit hyper-recombination, and purified RTEL1 unwinds D-loop HR intermediates,[38] suggesting an anti-recombinase function of RTEL1. In addition to its role in telomere maintenance and HR, RTEL1 interacts with PCNA and facilitates genome-wide replication.[39] Disruption of RTEL1-PCNA interaction in mouse cells causes accelerated senescence, reduced fork progression, increased origin usage, replication fork instability, and telomere fragility. Moreover, mice lacking RTEL1-PCNA interaction developed tumors in the p53 null background.[39] However, the mechanisms underlying replication defects, compromised telomere elongation, and early onset of tumorigenesis in RTEL1-deficient cells remain unclear.

Here, we identify the role of RTEL1 in regulating RAD51-mediated HR and fork reversal activity during DNA replication. RTEL1 and HR factors localize predominantly to stalled replication forks. RAD51 promotes elevated recombination and fork reversal events during DNA replication in the absence of RTEL1. Co-depletion of RAD51, RAD51 paralogs, and fork remodelers such as SMARCAL1/ZRANB3/HLTF/FBH1 rescues the replication defect in RTEL1-deficient cells. Expression of HR and fork reversal defective mutants of RAD51 also rescues replication defects in RTEL1-depleted cells. RTEL1 helicase activity and its interaction with PCNA are required for controlling HR and facilitating normal DNA replication. Collectively, our data suggest that RTEL1 suppresses RAD51-mediated aberrant HR activity and prevents excessive fork remodeling during DNA replication to promote error-free genome duplication.

RESULTS

RTEL1 is required for genome-wide replication in human cells

Earlier studies revealed that RTEL1 suppresses HR during DSB repair and contributes to genome-wide DNA replication.[37–41] However, the precise role of RTEL1 in human DNA replication remains elusive. To study this, we analyzed the sensitivity of RTEL1-depleted U2OS cells to the replication-stress-inducing agent hydroxyurea (HU) using two independent short hairpin RNAs (shRNAs). Compared to control cells, RTEL1-depleted cells were sensitive to HU but not DSB-inducing agent zeocin (Figures 1A, S1A, and S1B), suggesting the specific involvement of RTEL1 in the replication stress response pathway. To investigate the role of RTEL1 in global DNA replication, we performed BrdU and EdU incorporation assays in RTEL1-depleted cells using two independent shRNAs. Depletion of RTEL1 resulted in a significant reduction in BrdU and EdU incorporation as compared to control cells (Figures 1B and S1C–S1F). To study the kinetics of DNA replication at the single-molecule level, we performed DNA fiber analysis by sequential labeling of control and RTEL1-depleted cells with thymidine analogs CldU and IdU. Consistent with the BrdU and EdU incorporation assay, the replication rate was significantly reduced in RTEL1-depleted cells as compared to control cells, with a concomitant increase in fork asymmetry (Figures 1C and 1D). The reduced replication fork progression in RTEL1-depleted cells prompted us to study the dynamics of RTEL1 assembly at the active, stalled, and restarted replication forks. To investigate this, we employed the IdU iPOND (isolation of proteins on the nascent DNA) analysis. We treated HeLa Kyoto cells with 2 mM HU for 2 h to stall replication forks and released them into fresh media containing IdU for 30 min to allow fork recovery. Indeed, we found that RTEL1 is associated with active forks and enriched at stalled and restarted forks (Figure 1E). In addition, we found that HR-promoting factors, such as RAD51 and RAD51 paralogs, RAD51C and XRCC3, were enriched along with RTEL1 in stalled and fork recovery conditions (Figure 1E). Next, we performed DNA fiber analysis to further understand the role of RTEL1 in the restart of stalled forks. We labeled control and RTEL1-depleted cells with CldU, followed by treatment with 2 mM HU for 2 h and recovery in fresh media containing IdU to label the restarted forks. Indeed, RTEL1-depleted cells showed increased fork stalling (red-only fibers) and reduced fork restart (red and green fibers) (Figure 1F), which was associated with a concomitant increase in new origin firing (green-only fibers) (Figure 1F). Moreover, the length of the IdU tracts in the restarted forks was significantly reduced in RTEL1-depleted cells (Figure 1G), further supporting the notion that RTEL1 regulates fork restart following HU-induced fork stalling. However, depletion of RTEL1 did not result in fork degradation after prolonged treatment with HU, suggesting that fork protection is unperturbed (Figure S1G). Taken together, our results establish an important role of RTEL1 in the regulation of mammalian DNA replication.

RTEL1 suppresses hyper-recombination during replication

RTEL1 is known to regulate HR events by promoting the synthesis-dependent strand annealing pathway.[38] As our iPOND analysis showed the association of several HR factors with

(C) (Top) Representative DNA fiber images to show fork slowdown in control and RTEL1-depleted U2OS cells. (Bottom) Analysis of replication rate in control and RTEL1-depleted U2OS cells. Data are represented as mean ± SEM from three independent experiments. A minimum of 100 fibers were scored for each condition. Mann-Whitney test, $*p < 0.05$, $**p < 0.01$, $***p < 0.001$, and $****p < 0.0001$. n.s., nonsignificant.
(D) (Top) Representative DNA fiber images showing fork asymmetry. (Bottom) Quantification of fork asymmetry ($n = 32$) in control and RTEL1-depleted U2OS cells from three independent experiments. Mann-Whitney test, $*p < 0.05$, $**p < 0.01$, $***p < 0.001$, and $****p < 0.0001$. n.s., nonsignificant.
(E) (Top) A schematic of the iPOND experiment. (Bottom) Western blot showing enrichment of RTEL1 and HR factors at active, stalled, and restarting forks by IdU-iPOND experiment. IdU immunoprecipitation (IP) was performed, and eluates were resolved by SDS-PAGE and blotted with indicated antibodies.
(F) (Top) A schematic of fork restart assay. Representative DNA fibers showing fork stalling, restarting, and new origin firing. The bar graph represents the percentage of stalled and restarted forks in control and RTEL1-depleted U2OS cells. The percentage of new origin firing events is also indicated. Data are represented as mean ± SD from three independent experiments. Unpaired t test, $*p < 0.05$, $**p < 0.01$, $***p < 0.001$, and $****p < 0.0001$. n.s., nonsignificant.
(G) (Left) Representative DNA fibers showing the length of IdU tracts in the restarted forks. (Right) Quantification of IdU tract lengths representing fork restart. A minimum of 100 fibers were scored for each condition. Data are represented as mean ± SEM from three independent experiments. Mann-Whitney test, $*p < 0.05$, $**p < 0.01$, $***p < 0.001$, and $****p < 0.0001$. n.s., nonsignificant.

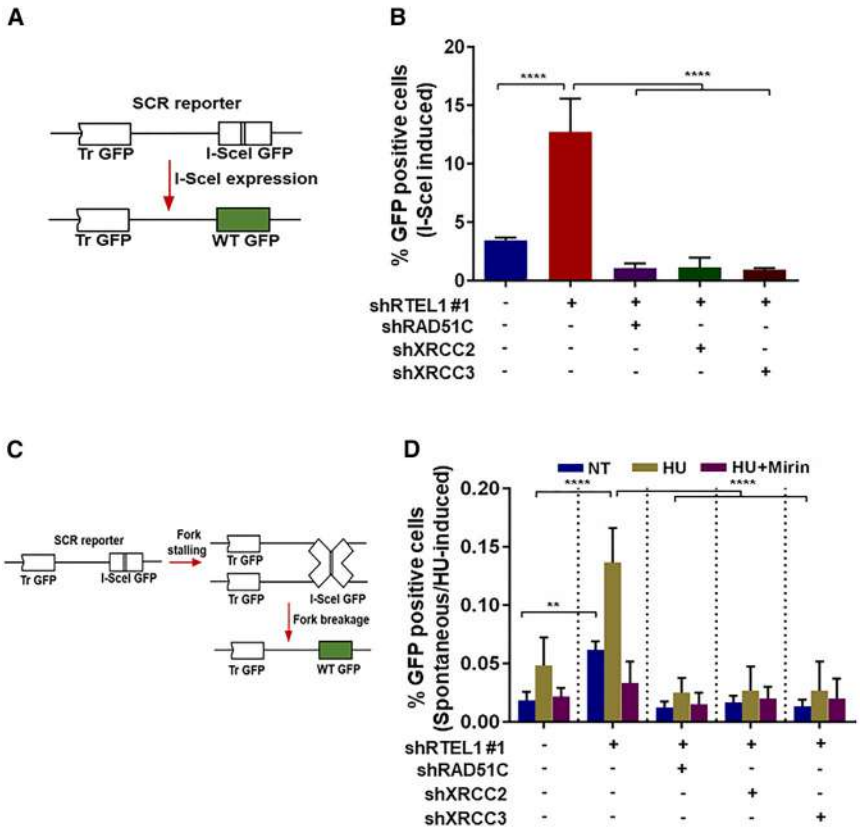

Figure 2. RTEL1 deficiency leads to elevated recombination events during DNA replication

(A) A schematic of SCR (sister chromatid recombination) reporter.

(B) I-SceI-induced HR frequencies in control, RTEL1 alone, and RTEL1 with indicated RAD51 paralogs co-depleted U2OS SCR18 cells. One-way ANOVA test, $*p < 0.05$, $**p < 0.01$, $***p < 0.001$, and $****p < 0.0001$. n.s., nonsignificant. Data are represented as mean ± SD from three independent experiments.

(C) A schematic of SCR reporter depicting replication-associated recombination. Prolonged fork stalling in the vicinity of the I-SceI restriction enzyme site leads to fork collapsing into breaks.

(D) Spontaneous and HU-induced HR frequencies in U2OS SCR18 control, RTEL1 alone, and indicated RAD51 paralog co-depleted cells. One-way ANOVA test, $*p < 0.05$, $**p < 0.01$, $***p < 0.001$, and $****p < 0.0001$. n.s., nonsignificant. Data are represented as mean ± SD from a minimum of three independent experiments.

stalled and restarted forks along with RTEL1 (Figure 1E), we speculated that RTEL1 might be involved in maintaining a balance of HR-promoting factors at the replication forks. In such a scenario, depletion of HR factors such as RAD51 paralogs might rescue the hyper-recombination phenotype associated with RTEL1 loss. To test this, we measured HR using sister chromatid recombination (SCR) reporter, which uses an I-SceI restriction enzyme to induce DSBs.[15] As expected, RTEL1-depleted cells showed an ~4-fold increase in HR events (Figures 2A, 2B, S2A, and S2B). Co-depletion of RAD51C, XRCC2, and XRCC3 in RTEL1 depletion background significantly abrogated HR frequencies (Figures 2B, S2A, and S2B). Next, we employed the SCR reporter to study the frequency of HR at stalled replication forks in the absence of I-SceI-induced DSBs, as studied earlier.[42] The generation of replication-associated breaks in the vicinity of the I-SceI site results in spontaneous HR events. Prolonged replication stress induced by a low dose of HU (100 μM) led to a low frequency of HU-induced HR events in the cells treated with control shRNA. However, there was a significant increase in HU-induced HR events in RTEL1-depleted cells (Figures 2C and 2D). Importantly, depletion of RAD51 paralogs in RTEL1-depleted cells prevented the elevated recombination frequency (Figure 2D), suggesting that RTEL1 limits HR at both DSBs and stalled replication forks. Stalled forks collapse upon prolonged exposure with HU, leading to the formation of single-ended DSBs.[24,43] HR is an important pathway for the restart of replication from the replication-associated DSBs, which involves MRE11-dependent processing.[43] In agreement with this, treatment with MRE11 inhibitor mirin abolished HU-induced elevated HR frequency in RTEL1-depleted cells (Figure 2D). Inhibition of MRE11 with mirin also rescued replication defects in RTEL1-depleted cells (Figures S2C and S2D). Together, our results highlight the key role of RTEL1 in regulating recombination events at both programmed and replication-associated DSBs.

RTEL1 helicase restricts HR to facilitate global DNA replication

Prompted by the elevated HR levels in RTEL1-depleted cells, we speculated that RTEL1 might be acting as a replisome-associated anti-recombinase to limit HR at stalled replication forks, thereby preventing global deregulation in replication. To understand whether elevated recombination events contribute to the replication defects in cells lacking RTEL1, we depleted RAD51 and RAD51 paralogs, RAD51C, XRCC2, and XRCC3, in the background of RTEL1 depletion and performed DNA fiber analysis (Figures 3A, 3B, and S3B). Interestingly, the reduced replication rate and elevated fork asymmetry in RTEL1-depleted cells were rescued by the depletion of RAD51 and RAD51 paralogs (Figures 3A–3D and S3A). In addition, co-depletion of RAD51 and RAD51 paralogs rescued the elevated frequency of stalled forks, promoting fork restart and preventing new origin firing in RTEL1-depleted cells (Figure 3E). We further analyzed the global replication by EdU incorporation in RTEL1 and RAD51 paralog co-depleted cells. Consistent with the DNA fiber assays, the reduced EdU incorporation in RTEL1-depleted cells was rescued by the co-depletion of RAD51C and XRCC2 (Figures 3F and S3C). Together, these data support the notion that aberrant HR at stalled replication forks leads to replication perturbations in cells lacking RTEL1.

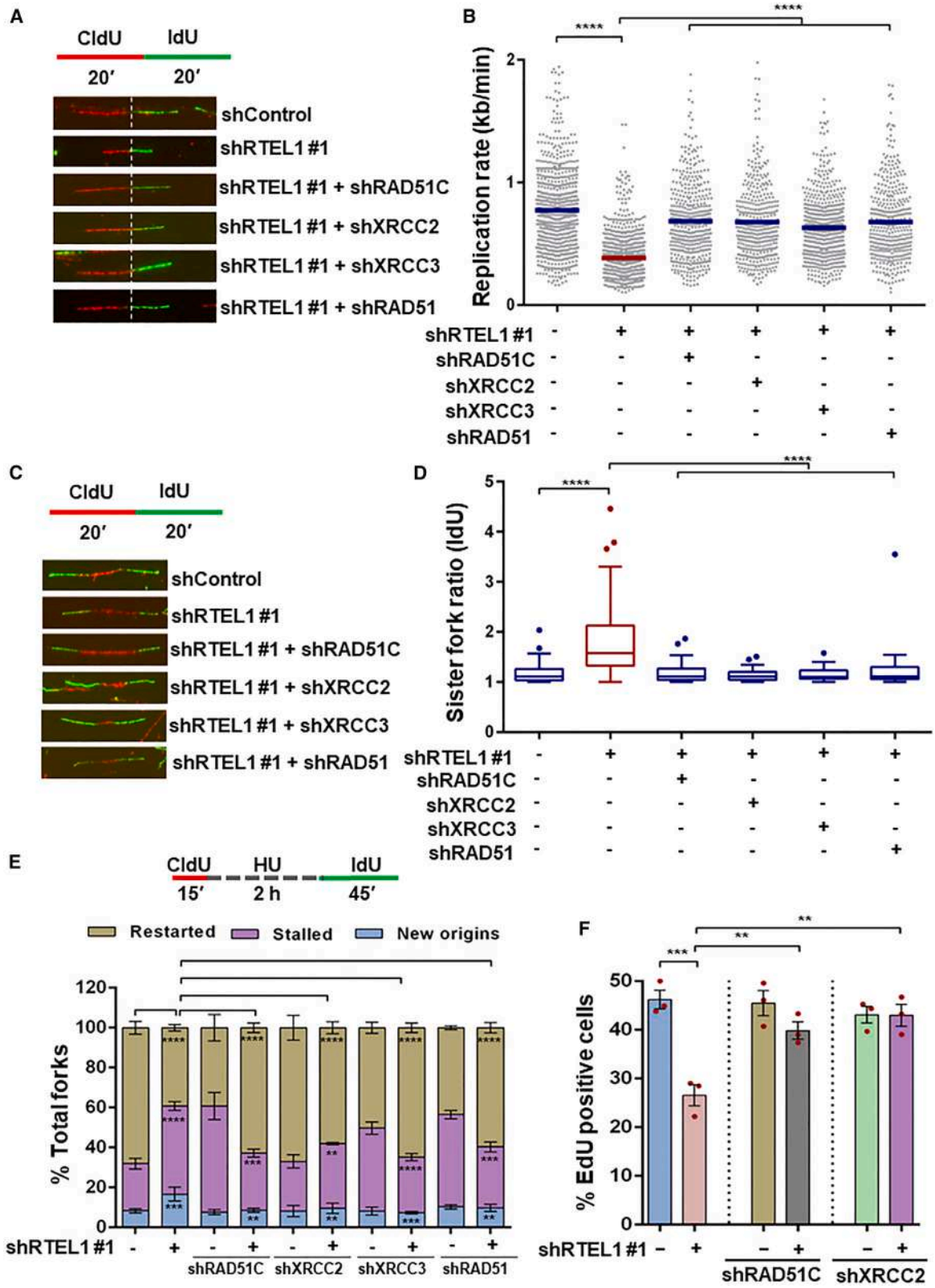

(legend on next page)

We have previously shown that RAD51 loading at DSBs and subsequent HR-mediated repair are dependent on XRCC3 phosphorylation.[44] Thus, we sought to investigate the effect of XRCC3 phosphorylation on DNA replication in RTEL1-depleted cells. To test this, we ectopically expressed shRNA-resistant wild-type (WT) XRCC3 and S225A XRCC3 in RTEL1 and XRCC3 co-depleted cells and analyzed replication tract lengths using DNA fibers. Notably, the expression of HR-deficient S225A XRCC3, but not HR-proficient WT XRCC3, rescued the reduced replication rate in RTEL1-depleted cells (Figures S4A–S4C), supporting the hypothesis that increased HR at stalled replication forks slows down replication. Further, fork asymmetry in RTEL1-depleted cells was significantly rescued upon expression of S225A XRCC3 but not with WT XRCC3 (Figure S4D).

Next, we investigated the involvement of the HR-specific function of XRCC2 in mediating continued replication in RTEL1-depleted cells. Previously, we reported that ATR-mediated XRCC2 phosphorylation at S247 is required for fork slowdown upon mild replication stress but is dispensable for RAD51 loading and repair of DSBs by HR.[25,45] Consistent with our hypothesis, the expression of HR-proficient WT and S247A XRCC2 could not rescue replication tract lengths and fork asymmetry in RTEL1-depleted cells (Figures S4E–S4H). Taken together, these results support the notion that aberrant recombination events at stalled replication forks in the absence of RTEL1 interfere with ongoing replication.

RTEL1 controls RAD51-mediated fork reversal

Replication fork reversal is a mechanism regulated by RAD51 in cooperation with multiple enzymes such as SMARCAL1, ZRANB3, HLTF, and FBH1, which actively slows down fork progression during replication stress and promotes the stabilization and repair of stalled forks.[46–54] We reasoned that the slow replication rate in RTEL1-depleted cells might be caused by unregulated fork reversal. To test this, we depleted SMARCAL1, ZRANB3, HLTF, and FBH1 in RTEL1-depleted cells (Figures S5A–S5D) and performed DNA fiber analysis. Interestingly, the reduced replication rates observed in RTEL1-depleted cells were significantly rescued by the depletion of SMARCAL1, ZRANB3, HLTF, and FBH1 (Figures 4A and 4B).

In addition to its DSB repair role, RAD51 recombinase promotes fork reversal and stabilizes stalled forks.[6,46] Interestingly, fork reversal by RAD51 is dependent on its HR activity.[55] Thus, we analyzed the role of RAD51 in the regulation of fork reversal and DNA replication in RTEL1-depleted cells. The strand exchange activity of RAD51 promotes fork reversal, wherein RAD51 II3A and T131P mutants devoid of strand exchange activity are unable to catalyze fork reversal.[55,56] The dominant-negative T131P RAD51 mutant protein interferes with proper RAD51 filament formation by the WT RAD51 proteins, thus inhibiting fork protection.[57] While the mutant protein itself cannot perform fork reversal, when co-expressed with WT RAD51, there is sufficient RAD51 function to promote reversal.[55,57] We expressed shRNA-resistant WT, II3A, and T131P RAD51 in RTEL1 and RAD51 co-depleted cells and analyzed replication rates using DNA fibers (Figure S5E). Interestingly, the reduced replication rate in RTEL1-depleted cells could not be rescued by the expression of T131P RAD51 mutant in cells with endogenous RAD51 (Figures 4C and 4D). However, the replication rate was significantly rescued when the T131P RAD51 mutant was expressed in the background of endogenous RAD51 depletion (Figure 4D). The expression of the strand-exchange-activity-deficient II3A RAD51 mutant in the RTEL1 alone and RTEL1 and RAD51 co-depleted cells resulted in a significant rescue of the replication rate compared to cells depleted of RTEL1 alone (Figure 4D). These data suggest that stalled forks in RTEL1-depleted cells undergo RAD51-mediated fork reversal, contributing to reduced replication rates.

RTEL1 inhibits accumulation of HR factors at the replicating sites

Many HR proteins, such as BRCA1/2, RAD51, and RAD51 paralogs, are involved in the protection of stalled replication forks.[5,24,26,58–60] To test whether RTEL1 is involved in regulating HR at stalled forks, we analyzed the enrichment of various HR-promoting factors at restarting replication forks using iPOND in control and cells lacking RTEL1. Interestingly, RAD51 and RAD51 paralogs (XRCC2 and XRCC3) were significantly enriched at restarting forks in RTEL1-depleted cells as compared to control cells (Figure 5A). In addition, nucleases such as SLX4 and MUS81 were abundant during recovery in RTEL1-depleted cells (Figure 5A), suggesting the collapse of stalled replication forks. Consistently, RTEL1-depleted cells showed increased phosphorylation of the XRCC3 S225 residue (Figure 5A). We then analyzed XRCC3 activation following an extended HU treatment that leads to replication fork stalling and, subsequently, collapse. Indeed, RTEL1-depleted cells showed early and increased activation of XRCC3 S225

Figure 3. Depletion of HR factors rescues replication defects in RTEL1-deficient U2OS cells

(A) A representative set of DNA fibers to display ongoing replication in indicated cells.

(B) Quantification of IdU tract lengths shown as replication rates (kb/min) in control, RTEL1 alone, and RTEL1 with indicated RAD51 paralog co-depleted cells. A minimum of 100 fibers were scored for each condition. Data are represented as mean ± SEM from three independent experiments. Mann-Whitney test, $*p < 0.05$, $**p < 0.01$, $***p < 0.001$, and $****p < 0.0001$. n.s., nonsignificant.

(C) Representative images of symmetric and asymmetric sister forks emanating from a single origin in indicated cells.

(D) Quantification of fork asymmetry in indicated cells from three independent experiments. $n \geq 27$ for asymmetric forks. Mann-Whitney test, $*p < 0.05$, $**p < 0.01$, $***p < 0.001$, and $****p < 0.0001$. n.s., nonsignificant.

(E) (Top) A schematic of fork restart assay. (Bottom) Bar graph represents percentage of fork stalling, fork restarting, and origin firing events in indicated U2OS cells. Data are represented as mean ± SD from three independent experiments. One-way ANOVA test, $*p < 0.05$, $**p < 0.01$, $***p < 0.001$, and $****p < 0.0001$. n.s., nonsignificant.

(F) Bar graph represents quantification of percentage of EdU incorporation in RTEL1 alone or RTEL1-combined RAD51C or XRCC2 -depleted U2OS cells. A minimum of 100 cells were counted for EdU incorporation from three independent experiments. One-way ANOVA test, $*p < 0.05$, $**p < 0.01$, $***p < 0.001$, and $****p < 0.0001$. n.s., nonsignificant. Data are represented as mean ± SEM.

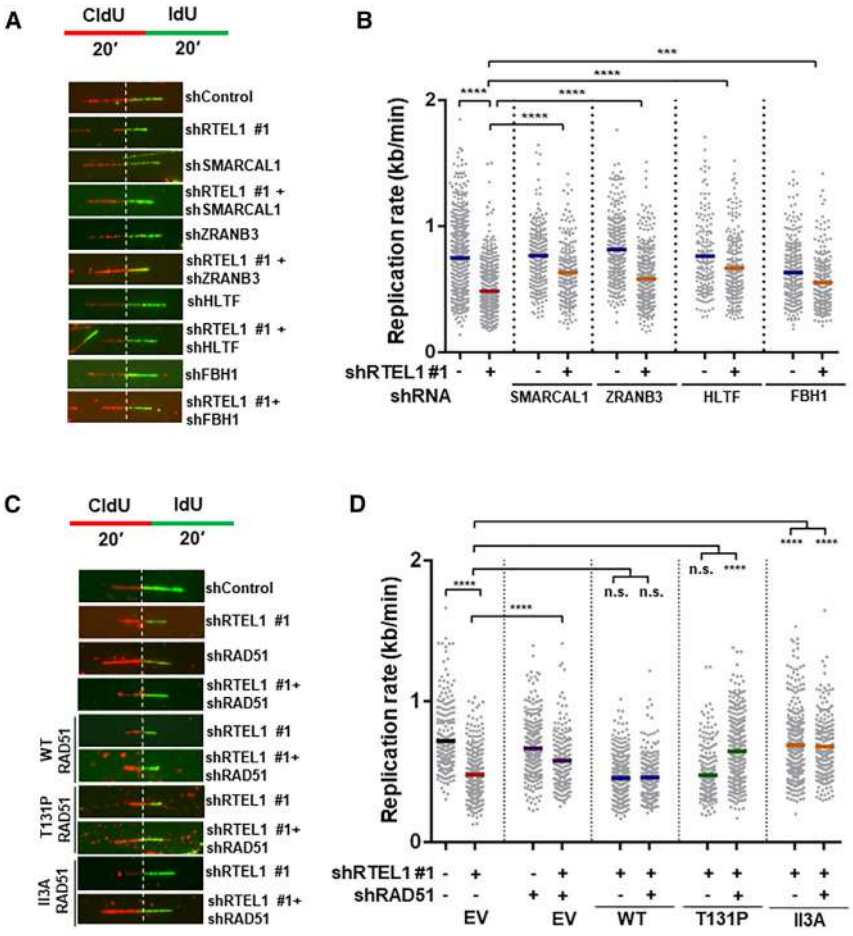

Figure 4. Depletion of fork remodelers and expression of HR-deficient RAD51 mutants rescues replication defects in RTEL1-depleted cells

(A) Representative DNA fiber images from control, RTEL1 alone, and RTEL1 with indicated fork reversal enzyme co-depleted U2OS cells.

(B) Quantification of IdU tract lengths shown as replication rates (kb/min) in indicated cells. A minimum of 100 fibers were scored for each condition from three independent experiments. Data are represented as mean ± SEM. Mann-Whitney test, $*p < 0.05$, $**p < 0.01$, $***p < 0.001$, and $****p < 0.0001$. n.s., nonsignificant.

(C) Representative DNA fiber images in indicated U2OS cells.

(D) Quantification of IdU tract lengths shown as replication rates (kb/min) in indicated cells. A minimum of 100 fibers were scored for each condition from three independent experiments. Data are represented as mean ± SEM. Mann-Whitney test, $*p < 0.05$, $**p < 0.01$, $***p < 0.001$, and $****p < 0.0001$. n.s., nonsignificant.

phosphorylation at 4 h of HU treatment analyzed by both western blotting (Figures S5F and S5G) and immunofluorescence (Figures S5H and S5I). In contrast, control cells showed an increase in XRCC3 phosphorylation only at 24 h of HU treatment, consistent with the generation of DSBs[43,44] (Figure S5F). RTEL1-depleted cells also showed increased phosphorylation of ATM targets CHK2 T68 and KAP1 S824 compared to control cells upon HU-induced replication stress (Figures S5J and S5K). This was consistent with the induction of DSBs as analyzed by neutral comet assay (Figures S5L and S5M), suggesting an early and increased collapse of stalled forks in RTEL1-depleted cells upon replication stress.

To validate our iPOND data demonstrating that HR factors persist at the stalled fork sites, we performed chromatin immunoprecipitation (ChIP) experiments to examine the accumulation of RAD51 and RAD51C at the FRA3B fragile site on chromosome 3. In support of our data with iPOND analysis, we find an ~3-fold enrichment of RAD51 and RAD51C at FRA3B loci in the absence of RTEL1 following HU-induced replication stress (Figure 5B). Similarly, RTEL1-depleted cells showed elevated RAD51 foci following HU treatment (Figures 5C and 5D). Importantly, HU-induced elevated RAD51 foci in RTEL1-depleted cells were rescued upon depletion of RAD51 paralogs (Figures 5C and 5D). Together, these results show that RAD51 paralogs and RAD51 are enriched at the replicating sites in the absence of RTEL1, leading to elevated RAD51-mediated HR and fork reversal impeding DNA replication.

Loss of RTEL1 results in increased DNA damage and genome instability.[33,37–39,61,62] In agreement with these studies, RTEL1-depleted cells showed increased γH2AX and 53BP1 foci at 4 and 12 h recovery from HU treatment as compared to control cells (Figures S6A–S6C). Control cells showed a considerable reduction in both the DNA damage markers at 12 h recovery. However, RTEL1 depletion resulted in persistent DNA damage, as observed by an increased number of γH2AX and 53BP1 foci compared to control cells (Figures S6A–S6C). We then sought to analyze the effect of the depletion of RAD51 paralogs on DNA damage and genome instability in RTEL1-depleted cells. Surprisingly, co-depletion of RTEL1 and RAD51 paralogs led to a further increase in γH2AX signal than single depletions upon HU-induced replication stress (Figures S6D and S6E). Moreover, the depletion of RAD51C and XRCC2 led to a significant increase in chromosomal aberrations in RTEL1-depleted cells following HU-induced replication stress (Figures S7A and S7B). In contrast, depletion of RAD51 or SMARCAL1 and ZRANB3 fork remodelers in the background of RTEL1-depleted cells rescued the induction of DSBs compared to cells depleted of RTEL1 alone in the unchallenged conditions (Figure S7C). Notably, the expression of RNaseH1 in the RTEL1-depleted cells reduced DNA damage significantly compared to control cells (Figure S7C).

The suppression of DNA damage by expression of RNaseH1 in the RTEL1-depleted cells prompted us to examine whether RNaseH1 overexpression rescues replication defects in RTEL1-depleted cells. To address this, we compared the tract lengths in RAD51-depleted and/or RNaseH1-expressing cells

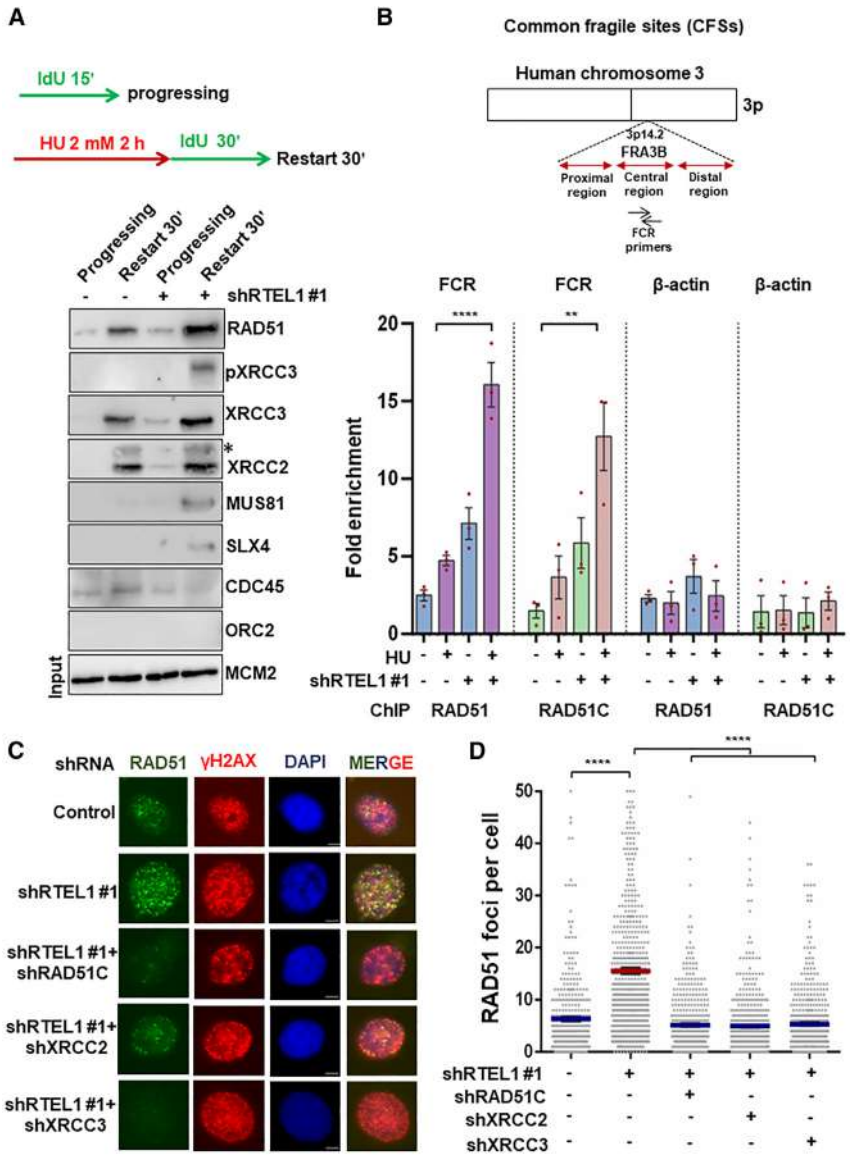

Figure 5. HR factors persist at the replicating sites in the absence of RTEL1

(A) (Top) A schematic of the IdU-iPOND experiment. (Bottom) Western blots showing enrichment of various HR factors at restarting forks (Restart 30′) in control and RTEL1-depleted HeLa cells by iPOND. HeLa cells were treated with 2 mM HU for 2 h followed by recovery in IdU-containing media. IdU IP was performed, and eluates were resolved by SDS-PAGE and blotted with indicated antibodies. * indicates a nonspecific band.

(B) (Top) A schematic showing genome organization of the FRA3B region. (Bottom) Fold enrichment of RAD51 and RAD51C at fragile site locus FRA3B. Control and RTEL1-depleted HeLa Kyoto cells were treated with 2 mM HU for 4 h and subjected to chromatin IP (ChIP). Data from three independent experiments are represented as mean ± SEM. One-way ANOVA test, $*p < 0.05$, $**p < 0.01$, $***p < 0.001$, and $****p < 0.0001$. n.s., nonsignificant.

(C) Representative images of RAD51 foci in control, RTEL1 alone, and RTEL1 with indicated RAD51 paralogs in co-depleted U2OS cells. Cells were treated with 2mM HU for 12 h prior to immunofluorescence staining. Scale bar: 10 μm.

(D) Quantification of RAD51 foci per cell as shown in (C). A minimum of 100 cells were scored for each condition from three independent experiments. Data are represented as mean ± SEM. Mann-Whitney test, $*p < 0.05$, $**p < 0.01$, $***p < 0.001$, and $****p < 0.0001$. n.s., nonsignificant.

in the RTEL1 depletion background. Consistent with our results (Figures 3A and 3B), the depletion of RAD51 rescued the replication defect in RTEL1-depleted cells. Ectopic expression of RNaseH1 also rescued replication defects in RTEL1-depleted cells. Interestingly, co-depletion of RAD51 and expression of RNaseH1 in the RTEL1-depleted cells did not rescue the replication defect further compared to RAD51 co-depleted or RNaseH1-expressing RTEL1-deficient cells (Figure S7D).

RAD51 and RAD51 paralogs are involved in the protection of nascent tracts and the restart and repair of damaged forks.[5,24–26,44] However, our results suggest that limiting RAD51 and RAD51 paralogs at stalled forks by RTEL1 is important for uninterrupted replication. Hence, we set out to investigate whether the inhibition of HR provides a survival advantage to RTEL1-depleted cells upon replication stress. Consistent with our previous results (Figure S1A), RTEL1-depleted cells showed a significant increase in sensitivity to HU-induced replication stress compared to control cells (Figure S8A). Interestingly, co-depleting RAD51 or RAD51 paralogs with RTEL1 did not alter HU-induced cell survival compared to cells depleted of RTEL1 alone (Figure S8A). These data suggest that limiting RAD51 is not sufficient to restore HU-induced cell survival in RTEL1-depleted cells. Together, our results suggest that the balance of RTEL1 and RAD51 activity at the fork is required to prevent genome instability arising due to replication stress.

PCNA interaction and helicase activity of RTEL1 is essential for regulating HR during replication

The RTEL1 is a 5′→3′ polarity helicase with an N-terminal helicase domain and a C-terminal PIP (PCNA interacting protein) motif[33] (Figure 6A). We investigated the involvement of the PIP motif of RTEL1 in the regulation of recombination events by generating the I1181A RTEL1 mutant. This mutant fails to interact with PCNA and exhibits a replication defect.[39] Strikingly, expression of the I1181A RTEL1 mutant failed to rescue the I-SceI and HU-induced recombination frequencies in RTEL1-depleted cells (Figures 6B, 6C, and S8B). In a parallel experiment, we also examined the helicase-defective Walker motif mutants of RTEL1 (K48A, ATP binding deficient and K48R, ATP

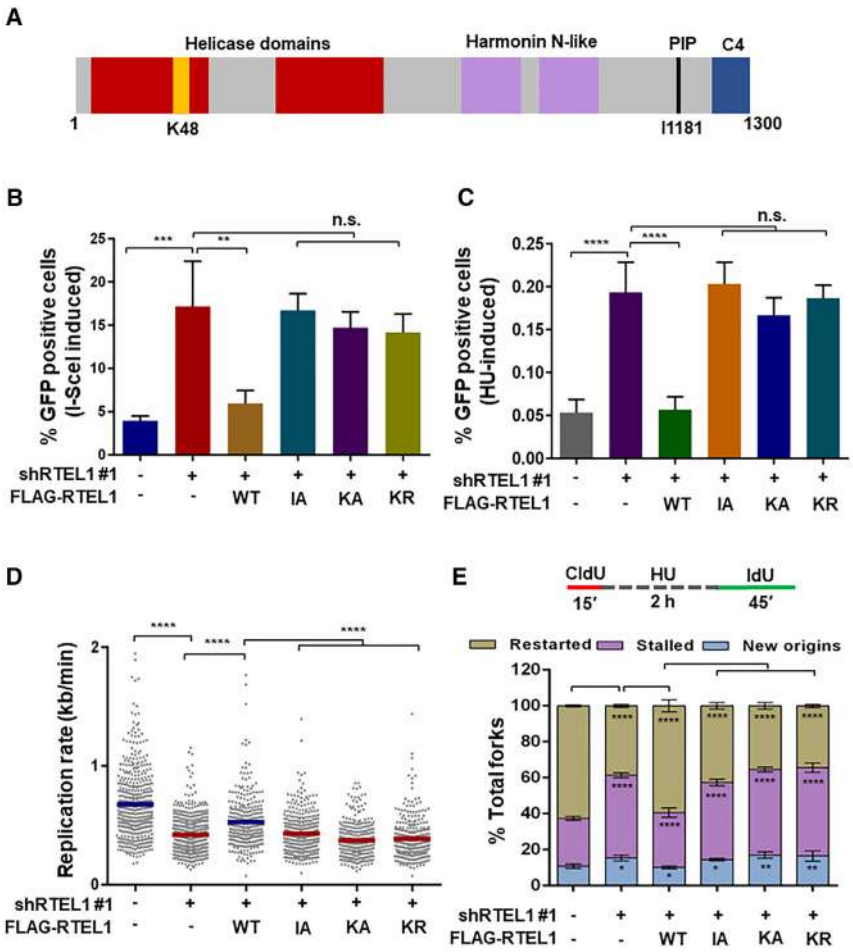

Figure 6. RTEL1 PCNA interaction and its helicase activity are required for suppressing HR during replication

(A) Domain architecture of RTEL1 helicase.

(B) I-SceI-induced HR frequencies in indicated U2OS SCR18 cells from three independent experiments. Data are represented as mean ± SD. One-way ANOVA test, $^{*}p < 0.05$, $^{**}p < 0.01$, $^{***}p < 0.001$, and $^{****}p < 0.0001$. n.s., nonsignificant.

(C) HU-induced HR frequencies in control, RTEL1 alone and RTEL1-depleted U2OS SCR18 cells expressing indicated RTEL1 mutants. Data are represented as mean ± SD from three independent experiments. One-way ANOVA test, $^{*}p < 0.05$, $^{**}p < 0.01$, $^{***}p < 0.001$, and $^{****}p < 0.0001$. n.s., nonsignificant.

(D) Quantification of IdU tract lengths shown as replication rates (kb/min) in indicated U2OS cells. A minimum of 100 fibers were scored for each condition from three independent experiments. Data are represented as mean ± SEM. Mann-Whitney test, $^{*}p < 0.05$, $^{**}p < 0.01$, $^{***}p < 0.001$, and $^{****}p < 0.0001$. n.s., nonsignificant.

(E) (Top) A schematic of fork restart assay. (Bottom) Bar graph represents percentage of stalled forks, restarted forks, and origin firing events in indicated U2OS cells from three independent experiments. Data are represented as mean ± SD. One-way ANOVA test, $^{*}p < 0.05$, $^{**}p < 0.01$, $^{***}p < 0.001$, and $^{****}p < 0.0001$. n.s., nonsignificant.

binding competent but hydrolysis deficient).[38,62] Notably, the expression of helicase dead mutants of RTEL1 failed to rescue I-SceI as well as HU-induced hyper-HR in RTEL1-depleted cells (Figures 6B, 6C, and S8B), suggesting that ATP binding and ATPase activity of RTEL1 are essential for its anti-recombinase function at both I-SceI-induced DSBs and stalled/collapsed replication forks.

Increased HU-induced recombination frequency observed upon the expression of RTEL1 helicase and PIP mutants could arise due to frequent fork stalling/collapse and might impair DNA replication. To test this, we examined the DNA replication rate in the PIP motif and helicase mutants of RTEL1-expressing cells in comparison with RTEL1-deficient cells by DNA fiber assay. Notably, the replication rate was significantly reduced in K48A and K48R RTEL1-expressing cells compared to WT RTEL1-expressing cells (Figures 6D and S8C), highlighting the role of helicase activity of RTEL1 in facilitating replication. Consistent with a previous report,[39] the I1181A RTEL1 mutant showed a defect in the DNA replication rate (Figures 6D and S8C). Notably, these replication defects can be rescued by co-depletion of RAD51 in the cells expressing RTEL1 I1181A, K48A, and K48R mutants (Figures S8D and S8E). To get further insights into RTEL1 mutants, we examined the frequency of stalled and restarted forks in RTEL1-depleted cells expressing RTEL1 I1181A, K48A, and K48R mutants. Similar to RTEL1-depleted cells, the expression of RTEL1 mutants resulted in an increased frequency of stalled forks and reduced restarted forks with a concomitant increase in new origin firing (Figure 6E). Together, our results demonstrate that RTEL1 helicase activity and its interaction with PCNA are important for regulating recombination at stalled replication forks and facilitating genome-wide replication.

DISCUSSION

RAD51, in addition to its canonical role in HR-mediated DSB repair, also participates in resolving replication problems during genome duplication, contributing to genome maintenance and tumor suppression.[2,9,13,63,64] Indeed, HR-defective cells exhibit impaired replication fork progression, fragile site expression, anaphase bridges, multipolar mitosis, and chromosome segregation defects.[65–68] RAD51 localizes to the stalled fork sites, promotes fork reversal, and stabilizes stalled forks from degradation by nucleases.[5,24,26,46,56,58–60,69] RAD51 also promotes the restart of stalled replication forks by its HR activity and facilitates the recovery of broken forks by a break-induced replication (BIR) mechanism.[24,25,43,44,46,70] Nonetheless, unregulated HR during replication can lead to the accumulation of mutations and genome rearrangements.[27,71–74] The factors and mechanisms

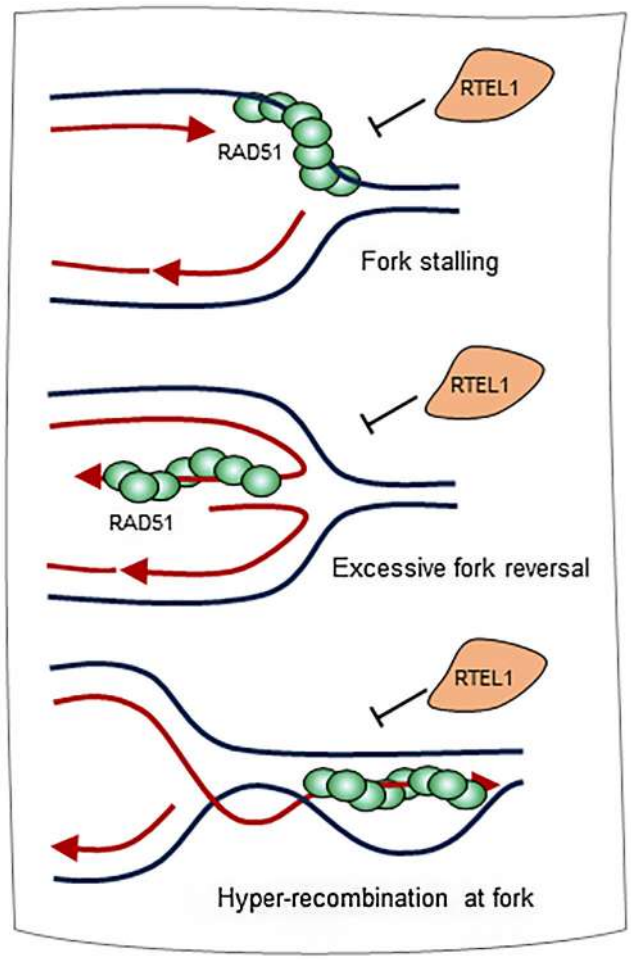

Figure 7. A model to explain RTEL1 functions at the replicating sites

RTEL1 regulates HR and fork reversal at stalled replication forks by limiting RAD51 accumulation. This activity of RTEL1 prevents excessive fork remodeling by RAD51 and RAD51-mediated hyper-HR.

underlying HR regulation and fork reversal activities by RAD51 during replication are less understood. Our data show that RTEL1 helicase suppresses unwarranted HR during genome duplication and prevents excessive fork remodeling by RAD51. Further, RTEL1-mediated RAD51 regulation is dependent on its helicase activity and interaction with PCNA.

RAD51, RAD51 paralogs, and RTEL1 helicase localize to the stalled forks after replication stress. The absence of RTEL1 leads to an increase in the frequency of HR at stalled forks, which can be rescued by the co-depletion of RAD51 and RAD51 paralogs. Strikingly, replication defects in RTEL1-depleted cells can also be rescued by the co-depletion of RAD51 or RAD51 paralogs. These data clearly show that unregulated HR impairs DNA replication, and RTEL1 helicase suppresses aberrant recombination events during normal DNA replication. Indeed, RAD51 and RAD51 paralogs persist at replicating sites in the RTEL1-deficient cells. The anti-recombinase function of RTEL1 has been shown in the context of DSB repair.[38] Data presented here extend RTEL1 helicase function in suppressing HR during genome duplication.

Stalled forks undergo remodeling to slow down DNA replication, and the reversed forks prevent nucleolytic degradation and facilitate the restart of stalled replication.[5–8] RAD51 promotes fork reversal by nucleating onto single-stranded DNA (ssDNA) at stalled forks and binds to reversed forks to prevent its degradation by nucleases.[46,60] In addition to RAD51, ATP-dependent DNA translocases such as SMARCAL1, ZRANB3, HLTF, and FBH1 also catalyze fork reversal.[47–54] These remodeling factors appear to participate in two distinct pathways to protect forks by different fork protection factors.[50] Interestingly, knockdown of either of these remodeling factors in the RTEL1-deficient cells significantly rescued global DNA replication, implying that fork reversal is one of the major causes of replication defects in RTEL1-depleted cells. It has been shown that fork reversal in RTEL1-deficient cells leads to telomere fragility, which can be prevented by inhibiting PARP1 and ZRANB3.[75] SMARCAL1, ZRANB3, and HLTF have nonredundant roles in promoting fork reversal.[48] In addition to RAD51, RAD51 paralogs (BCDX2 complex) have been implicated in facilitating fork reversal.[26,46] Nonetheless, it is unclear how RAD51 or RAD51 paralogs co-ordinate with these remodeling factors in driving fork reversal. Interestingly, the extent of the rescue of replication defects in RTEL1-deficient cells was greater upon RAD51 co-depletion than with the co-depletion of fork remodelers, suggesting that the role of RAD51 in fork slowing extends beyond fork reversal. Conceivably, RAD51 could load onto ssDNA regions at active or stalled forks and attempt to promote HR and impede DNA replication.

The expression of RAD51 T131P and RAD51 II3A mutants significantly rescued the replication defect in the RTEL1-deficient cells, providing mechanistic insights into the global reduction in DNA replication in RTEL1-depleted cells. RAD51 T131P cannot form stable filaments due to increased ATPase activity and is HR defective.[57] Strikingly, the RAD51 T131P mutant is defective in promoting fork reversal,[55] implying that strand exchange activity is required for fork reversal. The RAD51 II3A mutant, proficient in forming stable nucleoprotein filaments but defective in strand exchange and fork reversal activities,[55,56] also rescues replication defects in RTEL1-depleted cells. The fact that these mutants can rescue the replication defect in RTEL1-deficient cells indicates that RAD51-mediated fork reversal impairs DNA replication. RTEL1 may be required for disengaging RAD51 from the stalled fork sites to prevent excessive fork reversal (Figure 7). Indeed, BLM, RECQL5, FBH1, and PARI helicases have been shown to dismantle RAD51.[76–83] However, an *in vitro* study showed that RTEL1 dismantles the D-loop, an HR intermediate, and thereby suppresses HR, but RAD51 stripping activity was not found.[38]

RAD51 plays an important role in the restart of stalled forks by its recombinase function. The RAD51 filament generated at the reversed forks can invade homologous template DNA ahead of the fork and promote HR-mediated fork restart.[6,43,46,84] It has been estimated that ~25% of the stalled forks undergo reversal in the normal cells upon replication stress,[46] and this number may further increase in the absence of RTEL1 due to unregulated RAD51 activity at the replicating sites. As a result, RAD51 may

also attempt HR-mediated strand invasion ahead of the stalled forks, and such an aberrant HR might hamper replication in the absence of RTEL1 (Figure 7). When the stalled fork collapses into breaks, RAD51 polymerizes onto the processed one-ended DSBs, invades the sister chromatid to generate D-loop structures, and facilitates replication restart by BIR.[12,43,85–87] The BIR is an error-prone pathway, leading to mutations and chromosomal rearrangements.[12,87] Conceivably, RTEL1 may regulate HR and BIR at the stalled/collapsed fork sites by disrupting RAD51-mediated D-loops.

The RADX protein that binds to ssDNA and RAD51 alleviates RAD51-mediated excessive fork remodeling.[88–90] Indeed, the unregulated fork remodeling by RAD51 and the replication defect in the absence of RADX can be rescued by co-depleting RAD51 or SMARCAL1, ZRANB3, and HLTF fork remodelers. Moreover, co-depletion of fork remodelers also rescued spontaneous accumulation of DSBs in RADX-depleted cells.[88,91,92] Similarly, co-depletion of fork remodelers rescued replication defects and suppressed the accumulation of spontaneous DNA damage in RTEL1-deficient cells. These observations corroborate with RADX restricting RAD51-mediated fork reversal. RADX stimulates RAD51 ATPase activity, disassembling RAD51 filaments from the fork sites.[92] In addition to RADX, RECQL5, PARI, and FBH1 helicases possess RAD51 dismantling activity and have been implicated as anti-recombinases.[78,79,81,82] However, RTEL1 lacks such activity, and the mechanism underlying RTEL1 regulation of RAD51 at stalled fork sites requires further studies. Moreover, whether RADX/PARI/FBH1/RECQL5 restrict RAD51 activity at the stalled/collapsed fork sites is unclear. In addition, whether any interplay exists between RTEL1 and RADX/PARI/FBH1/RECQL5 or whether these proteins function independently in controlling RAD51 function during replication needs further investigation.

RTEL1 plays an important role in preventing transcription-replication collisions (TRCs) by resolving G4 DNA structures and preventing R-loop accumulation.[37,62] The replication and survival defect in RTEL1-deficient cells was partially rescued by ectopic expression of RNaseH1.[37] Consistently, our data with overexpression of RNaseH1 in RTEL1-depleted cells showed a significant reduction in spontaneous DNA damage and replication defects. Interestingly, co-depletion of RAD51 and RNaseH1 expression in the RTEL1-depleted cells did not rescue the replication defect further compared to RAD51 co-depleted or RNaseH1-expressing RTEL1-deficient cells. This suggests that genome-wide fork reversal promoted by RAD51/fork remodelers and TRCs contributes to the same pathway, resulting in fork slowing in RTEL1-depleted cells. Indeed, a recent study shows that R-loop-induced stalled forks undergo fork remodeling, contributing to fork slowing.[93] Another study shows that RTEL1 interacts with SLX4 to facilitate DNA replication and prevents TRCs.[61] Our data demonstrate the role of RTEL1 in suppressing aberrant HR and excessive fork remodeling during replication. Preventing the accumulation of HR factors at stalled forks may be another mechanism by which RTEL1 inhibits TRCs to facilitate genome-wide replication. However, further studies are required to understand how RTEL1 regulates HR at R-loops or G4 DNA-induced stalled forks and even at the sites of TRCs.

Limitations of the study

Technically, with available tools, assessing how much HR is required for handling replication problems under normal conditions is difficult. The HR requirement might also vary depending on the lesions and nature of replication stress that every fork encounters. The current tools and techniques would not reveal this. Although the electron microscopy (EM) technique is the direct way of visualizing the fork reversal, in recent times, many groups have employed DNA fiber studies, taking a genetic approach to studying fork reversal. These studies are very convincing; hence, we have also taken a similar approach without performing EM studies. The endogenous levels of RTEL1 are low in the cells. At replicating sites, especially with stalled forks, ssDNA regions are abundantly exposed in the genome. IdU iPOND involves pulling down the proteins that are enriched on ssDNA and ssDNA-double-stranded DNA/fork junctions at the fork sites. We could demonstrate robust localization of RTEL1 at the replicating sites by IdU iPOND but not by EdU-iPOND. EdU-iPOND involves "click reactions" that are intrinsically harsh and work efficiently with proteins that have a higher affinity to nascent DNA/replisomes. Given that RTEL1 is a low-abundance as well as mechanistically highly dynamic protein with a potentially short half-life at the fork, it is challenging to robustly detect RTEL1 in EdU-iPOND. Indeed, RTEL1 was not identified by EdU-iPOND mass spectrometry analysis, and it was indicated as a false negative, suggesting low abundance at forks.[94]

STAR★METHODS

Detailed methods are provided in the online version of this paper and include the following:

- KEY RESOURCES TABLE
- RESOURCE AVAILABILITY
  - Lead contact
  - Materials availability
  - Data and code availability
- EXPERIMENTAL MODEL AND STUDY PARTICIPANT DETAILS
  - Cell lines
- METHOD DETAILS
  - DNA constructs and transfections
  - Immunostaining
  - HR assay
  - DNA fiber analysis
  - BrdU incorporation and cell cycle analysis
  - Western blotting
  - IdU-iPOND assay
  - ChIP
  - Cell survival assay
  - Neutral comet assay
  - Metaphase analysis
- QUANTIFICATION AND STATISTICAL ANALYSIS

SUPPLEMENTAL INFORMATION

Supplemental information can be found online at https://doi.org/10.1016/j.celrep.2024.114594.

ACKNOWLEDGMENTS

We thank the IISc confocal microscopy and FACS facility for their help. Funding by the Department of Science and Technology (EMR/2015/001720 and CRG/2022/003533), the Department of Atomic Energy (58/14/03/2022-BRNS), the

Department of Biotechnology (BT/PR23498/BRB/10/1590/2017 and BT/PR45508/MED/30/2414/2022), the J.C. Bose fellowship (JCB/2021/000009), and the IISc-DBT partnership program (BT/PR27952/INF/22/212/2018) and infrastructure support provided by funding from DST and UGC are greatly acknowledged. S.D. was supported by CSIR and is currently supported by SERB; D.B. and S. Sahoo are supported by DST-INSPIRE and a CSIR fellowship, respectively; and T.N. is supported by a fellowship from IISc. S. Saxena was supported by a fellowship from IISc. K.S. was supported by a fellowship from CSIR, Bristol Meyers-Squibb fellowship, UK and Ranbaxy Science Foundation, India.

AUTHOR CONTRIBUTIONS

S.D., K.S., and G.N. conceived the project and designed the experiments. S.D., D.B., T.N., S. Saxena, and K.S. performed the experiments. S. Sahoo contributed to the generation of reagents. S.D., D.B., T.N., K.S., and G.N. analyzed the data. S.D., S. Saxena, K.S., and G.N. wrote the manuscript. R.K.C. facilitated the funding support from DAE.

DECLARATION OF INTERESTS

The authors declare no competing interests.

Received: October 5, 2023
Revised: May 23, 2024
Accepted: July 22, 2024

REFERENCES

1. Saxena, S., and Zou, L. (2022). Hallmarks of DNA replication stress. Mol. Cell. *82*, 2298–2314.
2. Zeman, M.K., and Cimprich, K.A. (2014). Causes and consequences of replication stress. Nat. Cell Biol. *16*, 2–9.
3. Nagaraju, G., and Scully, R. (2007). Minding the gap: the underground functions of BRCA1 and BRCA2 at stalled replication forks. DNA Repair *6*, 1018–1031.
4. Cortez, D. (2019). Replication-Coupled DNA Repair. Mol. Cell. *74*, 866–876.
5. Bhattacharya, D., Sahoo, S., Nagraj, T., Dixit, S., Dwivedi, H.K., and Nagaraju, G. (2022). RAD51 paralogs: Expanding roles in replication stress responses and repair. Curr. Opin. Pharmacol. *67*, 102313.
6. Berti, M., Cortez, D., and Lopes, M. (2020). The plasticity of DNA replication forks in response to clinically relevant genotoxic stress. Nat. Rev. Mol. Cell Biol. *21*, 633–651.
7. Berti, M., and Vindigni, A. (2016). Replication stress: getting back on track. Nat. Struct. Mol. Biol. *23*, 103–109.
8. Rickman, K., and Smogorzewska, A. (2019). Advances in understanding DNA processing and protection at stalled replication forks. J. Cell Biol. *218*, 1096–1107.
9. Chakraborty, S., Schirmeisen, K., and Lambert, S.A. (2023). The multifaceted functions of homologous recombination in dealing with replication-associated DNA damages. DNA Repair *129*, 103548.
10. Scully, R., Panday, A., Elango, R., and Willis, N.A. (2019). DNA double-strand break repair-pathway choice in somatic mammalian cells. Nat. Rev. Mol. Cell Biol. *20*, 698–714.
11. Tubbs, A., and Nussenzweig, A. (2017). Endogenous DNA Damage as a Source of Genomic Instability in Cancer. Cell *168*, 644–656.
12. Epum, E.A., and Haber, J.E. (2022). DNA replication: the recombination connection. Trends Cell Biol. *32*, 45–57.
13. Branzei, D., and Foiani, M. (2010). Maintaining genome stability at the replication fork. Nat. Rev. Mol. Cell Biol. *11*, 208–219.
14. Nagaraju, G., Hartlerode, A., Kwok, A., Chandramouly, G., and Scully, R. (2009). XRCC2 and XRCC3 regulate the balance between short- and long-tract gene conversions between sister chromatids. Mol. Cell Biol. *29*, 4283–4294.
15. Nagaraju, G., Odate, S., Xie, A., and Scully, R. (2006). Differential regulation of short- and long-tract gene conversion between sister chromatids by Rad51C. Mol. Cell Biol. *26*, 8075–8086.
16. Somyajit, K., Subramanya, S., and Nagaraju, G. (2012). Distinct roles of FANCO/RAD51C protein in DNA damage signaling and repair: implications for Fanconi anemia and breast cancer susceptibility. J. Biol. Chem. *287*, 3366–3380.
17. Venkitaraman, A.R. (2009). Linking the cellular functions of BRCA genes to cancer pathogenesis and treatment. Annu. Rev. Pathol. *4*, 461–487.
18. Kass, E.M., Moynahan, M.E., and Jasin, M. (2016). When Genome Maintenance Goes Badly Awry. Mol. Cell. *62*, 777–787.
19. Zhao, W., Wiese, C., Kwon, Y., Hromas, R., and Sung, P. (2019). The BRCA Tumor Suppressor Network in Chromosome Damage Repair by Homologous Recombination. Annu. Rev. Biochem. *88*, 221–245.
20. Somyajit, K., Subramanya, S., and Nagaraju, G. (2010). RAD51C: a novel cancer susceptibility gene is linked to Fanconi anemia and breast cancer. Carcinogenesis *31*, 2031–2038.
21. Ait Saada, A., Lambert, S.A.E., and Carr, A.M. (2018). Preserving replication fork integrity and competence via the homologous recombination pathway. DNA Repair *71*, 135–147.
22. Spies, J., Polasek-Sedlackova, H., Lukas, J., and Somyajit, K. (2021). Homologous Recombination as a Fundamental Genome Surveillance Mechanism during DNA Replication. Genes *12*, 1960.
23. Guh, C.L., Lei, K.H., Chen, Y.A., Jiang, Y.Z., Chang, H.Y., Liaw, H., Li, H.W., Yen, H.Y., and Chi, P. (2023). RAD51 paralogs synergize with RAD51 to protect reversed forks from cellular nucleases. Nucleic Acids Res. *51*, 11717–11731.
24. Somyajit, K., Saxena, S., Babu, S., Mishra, A., and Nagaraju, G. (2015). Mammalian RAD51 paralogs protect nascent DNA at stalled forks and mediate replication restart. Nucleic Acids Res. *43*, 9835–9855.
25. Saxena, S., Dixit, S., Somyajit, K., and Nagaraju, G. (2019). ATR Signaling Uncouples the Role of RAD51 Paralogs in Homologous Recombination and Replication Stress Response. Cell Rep. *29*, 551–559.
26. Berti, M., Teloni, F., Mijic, S., Ursich, S., Fuchs, J., Palumbieri, M.D., Krietsch, J., Schmid, J.A., Garcin, E.B., Gon, S., et al. (2020). Sequential role of RAD51 paralog complexes in replication fork remodeling and restart. Nat. Commun. *11*, 3531.
27. Piazza, A., and Heyer, W.D. (2019). Homologous Recombination and the Formation of Complex Genomic Rearrangements. Trends Cell Biol. *29*, 135–149.
28. Carr, A.M., and Lambert, S. (2013). Replication stress-induced genome instability: the dark side of replication maintenance by homologous recombination. J. Mol. Biol. *425*, 4733–4744.
29. Al-Zain, A.M., and Symington, L.S. (2021). The dark side of homology-directed repair. DNA Repair *106*, 103181.
30. Guirouilh-Barbat, J., Lambert, S., Bertrand, P., and Lopez, B.S. (2014). Is homologous recombination really an error-free process? Front. Genet. *5*, 175.
31. Heyer, W.D., Ehmsen, K.T., and Liu, J. (2010). Regulation of homologous recombination in eukaryotes. Annu. Rev. Genet. *44*, 113–139.
32. Hourvitz, N., Awad, A., and Tzfati, Y. (2024). The many faces of the helicase RTEL1 at telomeres and beyond. Trends Cell Biol *34*, 109–121.
33. Vannier, J.B., Sarek, G., and Boulton, S.J. (2014). RTEL1: functions of a disease-associated helicase. Trends Cell Biol. *24*, 416–425.
34. Speckmann, C., Sahoo, S.S., Rizzi, M., Hirabayashi, S., Karow, A., Serwas, N.K., Hoemberg, M., Damatova, N., Schindler, D., Vannier, J.B., et al. (2017). Clinical and Molecular Heterogeneity of RTEL1 Deficiency. Front. Immunol. *8*, 449.

35. Vannier, J.B., Pavicic-Kaltenbrunner, V., Petalcorin, M.I.R., Ding, H., and Boulton, S.J. (2012). RTEL1 dismantles T loops and counteracts telomeric G4-DNA to maintain telomere integrity. Cell *149*, 795–806.

36. Björkman, A., Johansen, S.L., Lin, L., Schertzer, M., Kanellis, D.C., Katsori, A.M., Christensen, S.T., Luo, Y., Andersen, J.S., Elsässer, S.J., Londono-Vallejo, A., et al. (2020). Human RTEL1 associates with Poldip3 to facilitate responses to replication stress and R-loop resolution. Genes Dev. *34*, 1065–1074.

37. Kotsantis, P., Segura-Bayona, S., Margalef, P., Marzec, P., Ruis, P., Hewitt, G., Bellelli, R., Patel, H., Goldstone, R., Poetsch, A.R., and Boulton, S.J. (2020). RTEL1 Regulates G4/R-Loops to Avert Replication-Transcription Collisions. Cell Rep. *33*, 108546.

38. Barber, L.J., Youds, J.L., Ward, J.D., McIlwraith, M.J., O'Neil, N.J., Petalcorin, M.I.R., Martin, J.S., Collis, S.J., Cantor, S.B., Auclair, M., et al. (2008). RTEL1 maintains genomic stability by suppressing homologous recombination. Cell *135*, 261–271.

39. Vannier, J.B., Sandhu, S., Petalcorin, M.I.R., Wu, X., Nabi, Z., Ding, H., and Boulton, S.J. (2013). RTEL1 is a replisome-associated helicase that promotes telomere and genome-wide replication. Science *342*, 239–242.

40. Uringa, E.J., Lisaingo, K., Pickett, H.A., Brind'Amour, J., Rohde, J.H., Zelensky, A., Essers, J., and Lansdorp, P.M. (2012). RTEL1 contributes to DNA replication and repair and telomere maintenance. Mol. Biol. Cell *23*, 2782–2792.

41. Bellelli, R., Youds, J., Borel, V., Svendsen, J., Pavicic-Kaltenbrunner, V., and Boulton, S.J. (2020). Synthetic Lethality between DNA Polymerase Epsilon and RTEL1 in Metazoan DNA Replication. Cell Rep. *31*, 107675.

42. Saleh-Gohari, N., Bryant, H.E., Schultz, N., Parker, K.M., Cassel, T.N., and Helleday, T. (2005). Spontaneous homologous recombination is induced by collapsed replication forks that are caused by endogenous DNA single-strand breaks. Mol. Cell Biol. *25*, 7158–7169.

43. Petermann, E., Orta, M.L., Issaeva, N., Schultz, N., and Helleday, T. (2010). Hydroxyurea-stalled replication forks become progressively inactivated and require two different RAD51-mediated pathways for restart and repair. Mol. Cell. *37*, 492–502.

44. Somyajit, K., Basavaraju, S., Scully, R., and Nagaraju, G. (2013). ATM- and ATR-mediated phosphorylation of XRCC3 regulates DNA double-strand break-induced checkpoint activation and repair. Mol. Cell Biol. *33*, 1830–1844.

45. Saxena, S., Somyajit, K., and Nagaraju, G. (2018). XRCC2 Regulates Replication Fork Progression during dNTP Alterations. Cell Rep. *25*, 3273–3282.

46. Zellweger, R., Dalcher, D., Mutreja, K., Berti, M., Schmid, J.A., Herrador, R., Vindigni, A., and Lopes, M. (2015). Rad51-mediated replication fork reversal is a global response to genotoxic treatments in human cells. J. Cell Biol. *208*, 563–579.

47. Ciccia, A., Nimonkar, A.V., Hu, Y., Hajdu, I., Achar, Y.J., Izhar, L., Petit, S.A., Adamson, B., Yoon, J.C., Kowalczykowski, S.C., et al. (2012). Polyubiquitinated PCNA recruits the ZRANB3 translocase to maintain genomic integrity after replication stress. Mol. Cell. *47*, 396–409.

48. Taglialatela, A., Alvarez, S., Leuzzi, G., Sannino, V., Ranjha, L., Huang, J.W., Madubata, C., Anand, R., Levy, B., Rabadan, R., et al. (2017). Restoration of Replication Fork Stability in BRCA1- and BRCA2-Deficient Cells by Inactivation of SNF2-Family Fork Remodelers. Mol. Cell. *68*, 414–430.

49. Halder, S., Ranjha, L., Taglialatela, A., Ciccia, A., and Cejka, P. (2022). Strand annealing and motor driven activities of SMARCAL1 and ZRANB3 are stimulated by RAD51 and the paralog complex. Nucleic Acids Res. *50*, 8008–8022.

50. Liu, W., Krishnamoorthy, A., Zhao, R., and Cortez, D. (2020). Two replication fork remodeling pathways generate nuclease substrates for distinct fork protection factors. Sci. Adv. *6*, eabc3598.

51. Fugger, K., Mistrik, M., Neelsen, K.J., Yao, Q., Zellweger, R., Kousholt, A.N., Haahr, P., Chu, W.K., Bartek, J., Lopes, M., et al. (2015). FBH1 Catalyzes Regression of Stalled Replication Forks. Cell Rep. *10*, 1749–1757.

52. Bétous, R., Mason, A.C., Rambo, R.P., Bansbach, C.E., Badu-Nkansah, A., Sirbu, B.M., Eichman, B.F., and Cortez, D. (2012). SMARCAL1 catalyzes fork regression and Holliday junction migration to maintain genome stability during DNA replication. Genes Dev. *26*, 151–162.

53. Couch, F.B., Bansbach, C.E., Driscoll, R., Luzwick, J.W., Glick, G.G., Bétous, R., Carroll, C.M., Jung, S.Y., Qin, J., Cimprich, K.A., and Cortez, D. (2013). ATR phosphorylates SMARCAL1 to prevent replication fork collapse. Genes Dev. *27*, 1610–1623.

54. Bai, G., Kermi, C., Stoy, H., Schiltz, C.J., Bacal, J., Zaino, A.M., Hadden, M.K., Eichman, B.F., Lopes, M., and Cimprich, K.A. (2020). HLTF Promotes Fork Reversal, Limiting Replication Stress Resistance and Preventing Multiple Mechanisms of Unrestrained DNA Synthesis. Mol. Cell. *78*, 1237–1251.

55. Liu, W., Saito, Y., Jackson, J., Bhowmick, R., Kanemaki, M.T., Vindigni, A., and Cortez, D. (2023). RAD51 bypasses the CMG helicase to promote replication fork reversal. Science *380*, 382–387.

56. Mason, J.M., Chan, Y.L., Weichselbaum, R.W., and Bishop, D.K. (2019). Non-enzymatic roles of human RAD51 at stalled replication forks. Nat. Commun. *10*, 4410.

57. Wang, A.T., Kim, T., Wagner, J.E., Conti, B.A., Lach, F.P., Huang, A.L., Molina, H., Sanborn, E.M., Zierhut, H., Cornes, B.K., et al. (2015). A Dominant Mutation in Human RAD51 Reveals Its Function in DNA Interstrand Crosslink Repair Independent of Homologous Recombination. Mol. Cell. *59*, 478–490.

58. Schlacher, K., Christ, N., Siaud, N., Egashira, A., Wu, H., and Jasin, M. (2011). Double-strand break repair-independent role for BRCA2 in blocking stalled replication fork degradation by MRE11. Cell *145*, 529–542.

59. Schlacher, K., Wu, H., and Jasin, M. (2012). A distinct replication fork protection pathway connects Fanconi anemia tumor suppressors to RAD51-BRCA1/2. Cancer Cell *22*, 106–116.

60. Hashimoto, Y., Ray Chaudhuri, A., Lopes, M., and Costanzo, V. (2010). Rad51 protects nascent DNA from Mre11-dependent degradation and promotes continuous DNA synthesis. Nat. Struct. Mol. Biol. *17*, 1305–1311.

61. Takedachi, A., Despras, E., Scaglione, S., Guérois, R., Guervilly, J.H., Blin, M., Audebert, S., Camoin, L., Hasanova, Z., Schertzer, M., et al. (2020). SLX4 interacts with RTEL1 to prevent transcription-mediated DNA replication perturbations. Nat. Struct. Mol. Biol. *27*, 438–449.

62. Wu, W., Bhowmick, R., Vogel, I., Özer, Ö., Ghisays, F., Thakur, R.S., Sanchez de Leon, E., Richter, P.H., Ren, L., Petrini, J.H., et al. (2020). RTEL1 suppresses G-quadruplex-associated R-loops at difficult-to-replicate loci in the human genome. Nat. Struct. Mol. Biol. *27*, 424–437.

63. Ciccia, A., and Elledge, S.J. (2010). The DNA damage response: making it safe to play with knives. Mol. Cell. *40*, 179–204.

64. Somyajit, K., Spies, J., Coscia, F., Kirik, U., Rask, M.B., Lee, J.H., Neelsen, K.J., Mund, A., Jensen, L.J., Paull, T.T., et al. (2021). Homology-directed repair protects the replicating genome from metabolic assaults. Dev. Cell *56*, 461–477.

65. van Gent, D.C., Hoeijmakers, J.H., and Kanaar, R. (2001). Chromosomal stability and the DNA double-stranded break connection. Nat. Rev. Genet. *2*, 196–206.

66. Chan, Y.W., and West, S.C. (2018). A new class of ultrafine anaphase bridges generated by homologous recombination. Cell Cycle *17*, 2101–2109.

67. Wilhelm, T., Magdalou, I., Barascu, A., Técher, H., Debatisse, M., and Lopez, B.S. (2014). Spontaneous slow replication fork progression elicits mitosis alterations in homologous recombination-deficient mammalian cells. Proc. Natl. Acad. Sci. USA *111*, 763–768.

68. Daboussi, F., Courbet, S., Benhamou, S., Kannouche, P., Zdzienicka, M.Z., Debatisse, M., and Lopez, B.S. (2008). A homologous recombination defect affects replication-fork progression in mammalian cells. J. Cell Sci. *121*, 162–166.

69. Mijic, S., Zellweger, R., Chappidi, N., Berti, M., Jacobs, K., Mutreja, K., Ursich, S., Ray Chaudhuri, A., Nussenzweig, A., Janscak, P., and Lopes, M.

(2017). Replication fork reversal triggers fork degradation in BRCA2-defective cells. Nat. Commun. *8*, 859.

70. Petermann, E., and Helleday, T. (2010). Pathways of mammalian replication fork restart. Nat. Rev. Mol. Cell Biol. *11*, 683–687.
71. Willis, N.A., Rass, E., and Scully, R. (2015). Deciphering the Code of the Cancer Genome: Mechanisms of Chromosome Rearrangement. Trends Cancer *1*, 217–230.
72. Piazza, A., Wright, W.D., and Heyer, W.D. (2017). Multi-invasions Are Recombination Byproducts that Induce Chromosomal Rearrangements. Cell *170*, 760–773.
73. Lambert, S., Watson, A., Sheedy, D.M., Martin, B., and Carr, A.M. (2005). Gross chromosomal rearrangements and elevated recombination at an inducible site-specific replication fork barrier. Cell *121*, 689–702.
74. Lambert, S., and Carr, A.M. (2013). Replication stress and genome rearrangements: lessons from yeast models. Curr. Opin. Genet. Dev. *23*, 132–139.
75. Margalef, P., Kotsantis, P., Borel, V., Bellelli, R., Panier, S., and Boulton, S.J. (2018). Stabilization of Reversed Replication Forks by Telomerase Drives Telomere Catastrophe. Cell *172*, 439–453.
76. Huselid, E., and Bunting, S.F. (2020). The Regulation of Homologous Recombination by Helicases. Genes *11*, 498.
77. Patel, D.S., Misenko, S.M., Her, J., and Bunting, S.F. (2017). BLM helicase regulates DNA repair by counteracting RAD51 loading at DNA double-strand break sites. J. Cell Biol. *216*, 3521–3534.
78. Hu, Y., Raynard, S., Sehorn, M.G., Lu, X., Bussen, W., Zheng, L., Stark, J.M., Barnes, E.L., Chi, P., Janscak, P., et al. (2007). RECQL5/Recql5 helicase regulates homologous recombination and suppresses tumor formation via disruption of Rad51 presynaptic filaments. Genes Dev. *21*, 3073–3084.
79. Schwendener, S., Raynard, S., Paliwal, S., Cheng, A., Kanagaraj, R., Shevelev, I., Stark, J.M., Sung, P., and Janscak, P. (2010). Physical interaction of RECQ5 helicase with RAD51 facilitates its anti-recombinase activity. J. Biol. Chem. *285*, 15739–15745.
80. Bugreev, D.V., Yu, X., Egelman, E.H., and Mazin, A.V. (2007). Novel pro- and anti-recombination activities of the Bloom's syndrome helicase. Genes Dev. *21*, 3085–3094.
81. Simandlova, J., Zagelbaum, J., Payne, M.J., Chu, W.K., Shevelev, I., Hanada, K., Chatterjee, S., Reid, D.A., Liu, Y., Janscak, P., et al. (2013). FBH1 helicase disrupts RAD51 filaments in vitro and modulates homologous recombination in mammalian cells. J. Biol. Chem. *288*, 34168–34180.
82. Moldovan, G.L., Dejsuphong, D., Petalcorin, M.I.R., Hofmann, K., Takeda, S., Boulton, S.J., and D'Andrea, A.D. (2012). Inhibition of homologous recombination by the PCNA-interacting protein PARI. Mol. Cell. *45*, 75–86.
83. Symington, L.S., and Heyer, W.D. (2006). Some disassembly required: role of DNA translocases in the disruption of recombination intermediates and dead-end complexes. Genes Dev. *20*, 2479–2486.
84. Carr, A., and Lambert, S. (2021). Recombination-dependent replication: new perspectives from site-specific fork barriers. Curr. Opin. Genet. Dev. *71*, 129–135.
85. Pasero, P., and Vindigni, A. (2017). Nucleases Acting at Stalled Forks: How to Reboot the Replication Program with a Few Shortcuts. Annu. Rev. Genet. *51*, 477–499.
86. Lemaçon, D., Jackson, J., Quinet, A., Brickner, J.R., Li, S., Yazinski, S., You, Z., Ira, G., Zou, L., Mosammaparast, N., and Vindigni, A. (2017). MRE11 and EXO1 nucleases degrade reversed forks and elicit MUS81-dependent fork rescue in BRCA2-deficient cells. Nat. Commun. *8*, 860.
87. Liu, L., and Malkova, A. (2022). Break-induced replication: unraveling each step. Trends Genet. *38*, 752–765.
88. Dungrawala, H., Bhat, K.P., Le Meur, R., Chazin, W.J., Ding, X., Sharan, S.K., Wessel, S.R., Sathe, A.A., Zhao, R., and Cortez, D. (2017). RADX Promotes Genome Stability and Modulates Chemosensitivity by Regulating RAD51 at Replication Forks. Mol. Cell. *67*, 374–386.
89. Zhang, H., Schaub, J.M., and Finkelstein, I.J. (2020). RADX condenses single-stranded DNA to antagonize RAD51 loading. Nucleic Acids Res. *48*, 7834–7843.
90. Schubert, L., Ho, T., Hoffmann, S., Haahr, P., Guérillon, C., and Mailand, N. (2017). RADX interacts with single-stranded DNA to promote replication fork stability. EMBO Rep. *18*, 1991–2003.
91. Krishnamoorthy, A., Jackson, J., Mohamed, T., Adolph, M., Vindigni, A., and Cortez, D. (2021). RADX prevents genome instability by confining replication fork reversal to stalled forks. Mol. Cell. *81*, 3007–3017.
92. Adolph, M.B., Mohamed, T.M., Balakrishnan, S., Xue, C., Morati, F., Modesti, M., Greene, E.C., Chazin, W.J., and Cortez, D. (2021). RADX controls RAD51 filament dynamics to regulate replication fork stability. Mol. Cell. *81*, 1074–1083.
93. Chappidi, N., Nascakova, Z., Boleslavska, B., Zellweger, R., Isik, E., Andrs, M., Menon, S., Dobrovolna, J., Balbo Pogliano, C., Matos, J., et al. (2020). Fork Cleavage-Religation Cycle and Active Transcription Mediate Replication Restart after Fork Stalling at Co-transcriptional R-Loops. Mol. Cell. *77*, 528–541.
94. Wessel, S.R., Mohni, K.N., Luzwick, J.W., Dungrawala, H., and Cortez, D. (2019). Functional Analysis of the Replication Fork Proteome Identifies BET Proteins as PCNA Regulators. Cell Rep. *28*, 3497–3509.

STAR★METHODS

KEY RESOURCES TABLE

REAGENT or RESOURCE	SOURCE	IDENTIFIER
Antibodies		
Anti-RTEL1	Thermo Fisher Scientific	Cat# PA5-71331; RRID: AB_2690764
Anti-BrdU (BrdU incorporation)	BD Biosciences	Cat# 555627
Rat anti-BrdU (For fiber)	Abcam	Cat# ab6326; RRID: AB_305426
Donkey Anti-Rat Alexa Fluor® 594 (For fiber)	Abcam	Cat# ab150156; RRID: AB_2890252
Purified Mouse Anti-BrdU (For fiber)	BD Biosciences	Cat# 347580; RRID: AB_400326
Rabbit Anti-Mouse IgG H&L (Alexa Fluor® 488) (For fiber)	Abcam	Cat# ab150125
Anti- pKAP1 S824	Abcam	Cat# ab70369; RRID: AB_1209417
Anti- pCHK2 T68	Cell Signaling Technology	Cat# 2197
Anti-Mouse IgG F(ab′)$_2$ fragment–FITC	Sigma-Aldrich	Cat# F2883
Anti-FLAG tag	Sigma-Aldrich	Cat# F1804; RRID: AB_262044
Anti- H2AX (pS139)	BD Biosciences	Cat# 560443; RRID: AB_1645592
Anti-SMARCAL1	Abcam	Cat# ab-154226
Anti-HLTF	Santa Cruz	Cat# sc-398357
Anti-ZRANB3	Abcam	Cat# ab109595; RRID: AB_10866685
Anti-FBH1	Santa Cruz	Cat# sc-81563
Anti-53BP1	Novus	Cat# NB100-305B; RRID: AB_1659856
Anti- RAD51	Santa Cruz	Cat# sc-8349; RRID: AB_2253533
Anti-Tubulin	Santa Cruz	Cat# sc-5286; RRID: AB_628411
Anti- MCM3	Santa Cruz	Cat# sc-365616; RRID: AB_10846721
Anti-MCM2	Santa Cruz	Cat# sc-373702
Anti-RPA70	Abcam	Cat# ab79398; RRID: AB_1603759
Anti-HA tag	Roche	Cat# 10952100
Anti-RAD51C	Santa Cruz	Cat# sc-56214; RRID: AB_2238197
Anti-XRCC2	Santa Cruz	Cat# sc-365854; RRID: AB_10846464
Anti-XRCC3	Santa Cruz	Cat# sc-271714; RRID: AB_10708416
Anti-CDC45	Santa Cruz	Cat# sc-55568; RRID: AB_831145
Anti-ORC2	Santa Cruz	Cat# sc-398410
Anti-MUS81	Santa Cruz	Cat# sc-47692; RRID: AB_2147129
Anti-SLX4	Santa Cruz	Cat# sc-135225
Anti- pXRCC3 S225	Somyajit et al.[44]	N/A
mouse anti-rabbit IgG-HRP	Santa Cruz	Cat# sc-2357
m-IgGκ BP-HRP	Santa Cruz	Cat# sc-516102

(*Continued on next page*)

Continued

REAGENT or RESOURCE	SOURCE	IDENTIFIER
Anti-hRAD51 polyclonal antibody (ChIP analysis)	Abcam	Cat# ab-176458; RRID: AB_2665405
Anti-hRAD51C polyclonal antibody (ChIP analysis)	Abcam	Cat# ab-72063; RRID: AB_2177279
Chemicals, peptides, and recombinant proteins		
Hydroxyurea	Sigma-Aldrich	Cat# H8627
Zeocin	Thermo Fisher Scientific	Cat# R25001
5-Bromo-2′-deoxyuridine	Sigma-Aldrich	Cat# B5002
Mirin	Sigma-Aldrich	Cat# M9948
DAPI	Sigma-Aldrich	Cat# D8417
5-Chloro-2′-deoxyuridine	Sigma-Aldrich	Cat# C6891
5-Iodo-2′-deoxyuridine	Sigma-Aldrich	Cat# I7125
cOmplete™, Mini Protease Inhibitor Cocktail	Roche	Cat# 11836153001
PhosSTOP	Roche	Cat# 4906837001
Thiazolyl Blue Tetrazolium Bromide (MTT reagent)	Sigma-Aldrich	Cat# M2128
KaryoMAX™ Colcemid™ Solution	Thermo Fisher Scientific	Cat# 15212012
Agarose, low gelling temperature	Sigma-Aldrich	Cat# A9414
Protein-G Sepharose beads	Cytiva	Cat# GE17-0618-01
Propidium Iodide	Sigma-Aldrich	Cat# P4170
5-ethynyl-2′-deoxyuridine	Thermo Fisher Scientific	A10044
Vectasheild	Vector Labs	Cat# H-1000
L-Ascorbic acid	Sigma-Aldrich	Cat# A92902
Alexa Fluor™ 488 Azide	Thermo Fisher Scientific	Cat# A10266
Alexa Fluor™ 647 Azide	Thermo Fisher Scientific	Cat# A10277
Deposited data		
Raw imaging and western data	This paper	http://www.doi.org/10.17632/mrpw4tt7x9.1
Experimental models: Cell lines		
U2OS	ATCC	HTB-96; RRID:CVCL_0042
HeLa Kyoto	Sachin Kotak Lab	RRID: CVCL_1922
U2OS SCR18	Ralph Scully lab	N/A
Oligonucleotides		
RTEL1 #1 (5′- GAGAAGCCCTGAGCTA CCTTGGGGT -3′)	Sigma-Aldrich	N/A
RTEL1 #2 (5′-GACCATCAGTGCTTAC TAT-3′)	Sigma-Aldrich	N/A
RAD51C (5′-CACCTTCTGTTCAGC ACTAGA-3′)	Sigma-Aldrich	N/A
XRCC2 (5′-TTGCAACGACACAAAC TATAA-3′)	Sigma-Aldrich	N/A
XRCC3 (5′-GAATTATTGCTGCAATTAA-3′)	Sigma-Aldrich	N/A
RAD51 (5′-GAAGAAATTGGAAGAAGCT-3′)	Sigma-Aldrich	N/A
SMARCAL1 (5′-GCTTTGACCTTCTTA GCAAT-3′)	Sigma-Aldrich	N/A
ZRANB3 (5′-TGGTGTGTGTCAGCT CTGT-3′)	Sigma-Aldrich	N/A
HLTF (5′-GGAATATAATGTTAACGAT-3′)	Sigma-Aldrich	N/A
FBH1 (5′-AAACAAAACCTCGTCATTA-3′)	Sigma-Aldrich	N/A
RTEL1 primers (Refer to Table S2)	N/A	N/A

(*Continued on next page*)

Continued

REAGENT or RESOURCE	SOURCE	IDENTIFIER
RAD51 primers (Refer to Table S2)	N/A	N/A
Recombinant DNA		
pcDNA3β-FLAG WT RTEL1	This paper	N/A
pcDNA3β-FLAG I1181A RTEL1	This paper	N/A
pcDNA3β-FLAG K48A RTEL1	This paper	N/A
pcDNA3β-FLAG K48R RTEL1	This paper	N/A
pcDNA3β-FLAG WT RAD51 (shRAD51 resistant)	This paper	N/A
pcDNA3β-FLAG T131P RAD51 (shRAD51 resistant)	This paper	N/A
pcDNA3β-FLAG II3A RAD51 (shRAD51 resistant)	This paper	N/A
pcDNA3β-HA WT XRCC2 (shXRCC2#1 resistant)	Saxena et al.[45]	N/A
pcDNA3β-HA S247A XRCC2 (shXRCC2#1 resistant)	Saxena et al.[45]	N/A
pcDNA3β-HA S247D XRCC2 (shXRCC2#1 resistant)	Saxena et al.[45]	N/A
pcDNA3β-HA WT XRCC3 (shXRCC3#1 resistant)	Saxena et al.[25]	N/A
pcDNA3β-HA S225A XRCC3 (shXRCC3#1 resistant)	Saxena et al.[25]	N/A
Software and algorithms		
ImageJ (DNA fiber length analysis)	ImageJ Software	https://imagej.nih.gov/ij/
GraphPad Prism 6	GraphPad Software	https://www.graphpad.com/
CytExpert software version 2.5	Beckman Coulter	N/A
ChemiDoc™ MP Imaging System	Bio-Rad	Cat# 12003154
CometScore Pro	TriTec Corp	N/A
CFX Mastro software for qPCR	Bio-Rad	Bio-Rad

RESOURCE AVAILABILITY

Lead contact

Further information and requests for resources and reagents should be directed to and will be fulfilled by the lead contact, Ganesh Nagaraju (nganesh@iisc.ac.in).

Materials availability

All unique reagents generated in this study are available without restrictions, and requests can be made to lead contact.

Data and code availability

- Uncropped blots and microscopy images are available through Mendeley (http://www.doi.org/10.17632/mrpw4tt7x9.1).
- This paper does not report the original code.
- Any additional information required to reanalyze the data reported in this paper is available from the lead contact upon request.

EXPERIMENTAL MODEL AND STUDY PARTICIPANT DETAILS

Cell lines

Human U2OS cells were obtained from ATCC. U2OS SCR18 cells were a kind gift from Prof. Ralph Scully (Harvard Medical School, Boston). HeLa Kyoto cells were a kind gift from Prof. Sachin Kotak, IISc, Bangalore. The source and identifier of U2OS and HeLa Kyoto cell lines are listed in the key resources table. U2OS and HeLa Kyoto cells were grown in Dulbecco's modified Eagle's medium (DMEM) with high glucose with 10% FBS, glutamax supplement and penicillin/streptomycin at 37°C in humidified air incubator containing 5% CO_2.

METHOD DETAILS

DNA constructs and transfections

Short hairpin RNAs (shRNAs) were generated from previously reported siRNA sequences (Table S1) and cloned into pRS shRNA vector. Human C-terminal FLAG tagged WT RTEL1, PIP motif mutant, helicase mutants, sh-RNA resistant versions of WT RAD51 and RAD51 mutants were generated using PCR-based mutagenesis and cloned into pcDNA3β vector. Sequences of primers used for generation of constructs are listed in table (Table S2). Transient transfections were performed using Bio-Rad gene pulsar X cell (250 V and 950 μF). Cells were recovered in fresh media 6 h post transfection. Cells were harvested 30 h post transfection for depletion and over-expression.

Immunostaining

Exponentially growing U2OS cells were plated on sterile coverslips in 12 well plates. Pre-extraction was performed using 0.5% Triton X-100 in PBS on ice for 5 min. Cells were washed with 1X PBS and fixed with 3.7% formaldehyde in 1X PBS for 12 min at room temperature (RT). Click-iT EdU staining was performed as per the manufacturer's protocol (Thermo Fisher Scientific). Cells were treated with 10μM EdU for 30 min prior to fixation and pre-extraction. Cells were incubated with indicated primary antibodies for 2 h and respective secondary antibodies for 1 h at RT diluted in DMEM with 10% FBS with high glucose and glutamax supplement. After incubation with each antibody, cells were washed three times with 0.2% Tween 20 in 1X PBS. Cells were then stained with DAPI (1 μg/mL; Sigma-Aldrich) for 5 min before mounting onto slides. Slides were visualized using Olympus confocal microscope FV3000 and Apotome microscope (Zeiss Axio observer).

HR assay

HR assay was performed as described previously.[15] Briefly, U2OS SCR18 cells were transfected with indicated shRNAs, RTEL1 WT and RTEL1 mutant constructs. Cells were transfected with 20 μg of I-SceI plasmid 24 h post transfection. Later cells were harvested at 48 h and GFP+ cells were analyzed by FACS. The percentage of GFP+ cells was normalized with transfection efficiency (~75–80%). The spontaneous GFP+ percentage (0.02%) was subtracted from absolute GFP frequency to obtain I-SceI induced HR frequencies. For spontaneous HR events, the percentage of GFP+ cells was analyzed as mentioned above without I-SceI transfection. For HU-induced HR frequency, cells were transfected with indicated shRNAs and RTEL1 plasmid constructs and were subsequently treated with 100 μM HU for 24 h. Cells were treated with 10 μM mirin, 4 h prior to indicated HU treatment. Cells were harvested and GFP+ cells were scored by FACS using CytoFLEX flow cytometer (Beckman Coulter). The percentage of GFP+ cells was normalized with transfection efficiency.

DNA fiber analysis

Cells were seeded in six well plates after transfection at 2.5 X 10^5 cells/well. Cells were pulse labeled with 25 μM CldU followed by 250 μM IdU for the indicated time. Replication was halted by adding chilled 1X PBS. Cells were harvested and stretched onto glass slides in DNA lysis buffer (200 mM Tris HCl pH 7.4, 50 mM EDTA, 0.5% SDS). Fibers were fixed in a 3:1 ratio of methanol and acetic acid followed by denaturation in 2.5 M HCL for 1 h. After 3 washes in 1X PBS, slides were incubated in blocking buffer (2% BSA, 0.1% Tween 20 in PBS) for 45 min. Later, slides were incubated with primary antibodies for CldU and IdU; rat anti-BrdU antibody at 1:500 dilution (Abcam; ab6326) and anti-IdU antibody at 1:250 dilution in blocking solution (BD Biosciences; 347580) respectively. After 2.5 h, slides were washed 3 times with 0.2% Tween 20 PBS and incubated in blocking solution for 15 min in a humidified chamber. Slides were incubated with secondary antibodies Anti-rat Alexa Fluor 594 (Abcam; ab150156) and Anti-mouse Alexa Fluor 488 (Abcam; ab150125) at 1:300 dilution. After 3 washes with 0.1% Tween 20 PBS, slides were air-dried for 30 min in a slanted position. Slides were mounted with Vectasheild mounting medium (Vector Labs H-1000). Slides were imaged using apotome microscope (Zeiss Axio observer). A minimum of 100 fibers were quantified from three independent experiments using ImageJ software and *p*-values were calculated using GraphPad Prism software. The replication rate in unchallenged cells was calculated by dividing the length of the IdU tracts (in kb) with the time of IdU incubation (in minutes).

BrdU incorporation and cell cycle analysis

Cells were pulse labeled with 50 μM BrdU for 20 min. Cells were harvested and fixed in 70% ethanol at −20°C overnight. Cells were thawed, followed by denaturation in 2N HCl in 1X PBS containing 0.5% Triton X-100 for 30 min. After several 1X PBS washes, cells were resuspended in blocking buffer (0.5% BSA, 0.5% Triton X-100 in 1X PBS) for 30 min. Cells were incubated with anti-BrdU antibody (BD Biosciences; 347580) for 2 h at RT. Cells were washed in blocking buffer and incubated with FITC-conjugated anti-mouse antibody (Sigma; F2883) for 1 h at RT. After 2 washes with 1X PBS, cells were incubated with RNase A (100 μg/mL) and propidium iodide (PI) (50 μg/mL) for 20 min at RT. Cells were analyzed using CytoFLEX flow cytometer (Beckman Coulter). Aggregates were gated out and the percentage of cells in S-phase was calculated using CytExpert software version 2.5 (Beckman Coulter).

Western blotting

Cells were lysed in RIPA buffer (50 mM Tris-HCl [pH 8.0], 250 mM NaCl, 0.1% SDS, 1% NP-40) supplemented with protease inhibitor (cOmplete Protease Inhibitor Cocktail, Roche). 50 μg protein was loaded on SDS-PAGE gel and transferred onto PVDF membrane

using Bio-Rad transfer apparatus (Trans Blot SD semi dry transfer cell). The membranes were blocked using 5% skimmed milk in PBST (0.1% Tween 20 in 1X PBS). Membranes were incubated with indicated primary antibodies overnight in blocking solution at 4°C. After 3 washes with PBST, membranes were incubated with respective HRP-conjugated secondary antibodies for 1 h at RT. Membranes were washed with PBST for 3 times and developed with HRP substrate using Bio-Rad chemidoc.

IdU-iPOND assay

IdU iPOND assay was performed as described previously.[24] To induce fork stalling, exponentially growing HeLa Kyoto cells (~10 million cells) were treated with 2 mM HU for 2 h. After extensive washing with 1X PBS, cells were grown in a fresh medium containing IdU (100 μM) for 30 min to allow the restart of stalled replication forks. Cells were cross-linked with 1% formaldehyde for 20 min followed by treatment with 0.125 M glycine to quench the excessive formaldehyde. Cells were collected in 50 mL tubes and washed with chilled 1X PBS thrice. Cells were incubated in hypotonic buffer (10 mM HEPES [pH 7.0], 50 mM NaCl, 0.3 M sucrose, 0.5% Triton X-100) supplemented with protease and phosphatase inhibitor tablets (PhosSTOP, Roche) for 15 min on ice and centrifuged at 1500xg for 5 min to remove cytosolic fraction. Cells were then incubated in nuclear buffer (10 mM HEPES [pH 7.0], 150 mM NaCl, 1 mM EDTA, 0.5% NP-40) for 10 min on ice and centrifuged at 13000 rpm for 2 min to remove soluble nuclear fraction. The pellet was resuspended in lysis buffer (10 mM HEPES [pH 7.0], 500 mM NaCl, 1 mM EDTA, 1% NP-40) followed by sonication at low amplitude. Samples were centrifuged at 13000 rpm for 1 min and supernatant was collected as chromatin fraction. After protein estimation using Bradford's assay, 250 μg of chromatin was incubated with 5 μg IdU antibody (BD Biosciences; 347580) overnight at 4°C. Next day, samples were incubated with 20 μL of Protein-G Sepharose beads (Cytiva; GE17-0618-01) for 4 h. IP reaction was washed thrice with wash buffer (10 mM HEPES [pH 7.0], 200 mM NaCl, 1 mM EDTA, 0.5% NP-40) followed by incubation in 2x Laemmli buffer at 95°C for 10 min. After the final centrifugation, the supernatant was collected and loaded onto SDS-PAGE gel for western blot analysis.

ChIP

After indicated HU treatment, HeLa Kyoto cells were subjected to DNA protein crosslinking by crosslinking buffer (5mM HEPES [pH 7.9], 0.1 mM EDTA, 10 mM NaCl and 1.1% formaldehyde) for 15 min at RT in dark. Excess formaldehyde was quenched by incubating the cells with 125 mM glycine for 5 min at RT. Cells were washed several times with ice-cold 1X PBS. Cytoplasmic fraction was removed by incubating cells with cell lysis buffer (5 mM PIPES[pH 8.0], 85 mM KCl and 0.5% NP-40) for 10 min on ice. Later, cells were pelleted down and washed twice with 1X PBS containing 0.5% NP-40. The pellet was resuspended in lysis buffer (50 mM Tris-HCl [pH 8.0], 10 mM EDTA, 0.5% SDS) supplemented with protease inhibitor cocktail. The chromatin fraction was sonicated on ice (12 cycles of 30 s at low amplitude) to generate DNA fragments of length 200 bp to 800 bp. Lysates were then subjected to centrifugation at 12500*g* for 2 min, and the resulting supernatant was precleared with protein-A-sepharose beads blocked with 500 μg/mL BSA for 2 h at 4°C. For each ChIP, 15 μg of pre-cleared chromatin was incubated with 4 μg of RAD51 antibody (Abcam ab-176458) and 6 μg of RAD51C antibody (Abcam ab-72063). An equivalent amount of chromatin was taken as no antibody control. 50 μL of protein-A beads were added to the chromatin-antibody complex and incubated for 2 h at 4°C. The beads were washed for 5 min each with low salt buffer (0.1% SDS, 1% Triton X-100, 2 mM EDTA, 2 mM Tris-HCl [pH 8.0], 150 mM NaCl), high salt buffer (0.1% SDS, 1% Triton X-100, 2 mM EDTA, 2 mM Tris-HCl [pH 8.0], 500 mM NaCl), LiCl wash buffer (250 mM LiCl, 1% NP-40, 1% sodium deoxycholate, 1 mM EDTA, 10 mM Tris-HCl [pH 8.0]) and twice with TE buffer (10 mM Tris-HCl [pH 8.0], 1 mM EDTA). Finally, the chromatin was eluted with elution buffer (1% SDS, 100 mM NaHCO3). Elutes were de-crosslinked by adding NaCl to a final concentration of 300 mM and incubated overnight at 65°C. After incubation with RNase (0.1 mg/mL; Invitrogen, 12091-021) at 42°C for 1 h, eluates were digested with Proteinase K (0.1 mg/mL; Sigma, 70663-4) for 6 h at 55°C. DNA was purified by phenol-chloroform-isoamyl alcohol (PCI) extraction and ethanol precipitation. The isolated DNA was used as a template for qPCR analysis on a Bio-Rad CFX Opus 96 Real-time PCR system using iTaq Universal SYBR Green Supermix (Bio-Rad). Fold enrichment was calculated as follows: fold enrichment = $2^{-(CtIP- CtNo\ ab)}$, where Ct_{IP} and $Ct_{No\ ab}$ are mean threshold cycles of PCR done on DNA samples immunoprecipitated with specific antibody and no antibody control, respectively. The sequences of primers used for qPCR analyses are listed in Table S1.

Cell survival assay

After transfection, ~5000 cells per well were seeded in a 24-well plate. Later, cells were grown for 7–8 days after treatment with indicated DNA damaging agents. Cell survival was analyzed using MTT (0.1 mg/mL; Sigma-Aldrich, M2128) assay at 595 nm wavelength using microplate reader (VERSAmax). The percentage survival is represented as treated/untreated cells×100 from at least three independent experiments.

Neutral comet assay

Silane-Prep slides (Sigma; S4651) were coated with 0.8% agarose in 1X PBS at least 24 h before the experiment. Cells were treated with HU as mentioned and harvested in 1X PBS. After centrifugation, cells were resuspended in 200 μL of 0.7% LMP agarose in 1X PBS followed by spreading 65 μL of agarose containing cells on pre-coated slides. The slides were kept on icepack for solidification followed by coating with 0.7% LMP agarose. Slides were placed in chilled lysis buffer (2.5 M NaCl, 0.1 M EDTA, 100 mM Tris-HCl [pH 10.0], 1% N-laurylsarcosine, 0.5% Triton X-100, 10% DMSO) for 2 h at 4°C. Slides were then washed in electrophoresis buffer (300 mM sodium acetate, 100 mM Tris-HCl [pH 8.0]) for three times. Slides were transferred to electrophoresis tank filled with chilled

electrophoresis buffer. The electrophoresis was performed at 15 V (0.5 V/cm) for 1 h at RT. Slides were washed with 1X PBS twice, fixed in absolute ethanol for 30 min at RT. Slides were then air-dried and stained with PI (2 μg/mL in Milli-Q). Slides were imaged using Apotome microscope (Zeiss Axio observer). A minimum of 100 comets were scored using CometScore software from 3 independent experiments.

Metaphase analysis

After indicated transfections, cells were treated with 2 mM HU for 4 h followed by recovery in fresh media for 24 h. Cells were incubated with 0.1 μg/mL KaryoMAX Colcemid (Gibco; 15212012) for last 4 h of the recovery. Cells were harvested and resuspended in hypotonic solution (0.075 M KCl in Milli-Q) for 12 min at 37°C. Cells were pelleted down and fixed in 5 mL of fresh Carnoy's fixative (3:1 ratio of methanol: acetic acid). Cells were dropped onto chilled slides followed by incubation on a steaming water beaker (70°C-80°C) for 90 s. Slides were then air-dried, stained with Geimsa (Sigma; GS500) at 1:20 dilution for 30 min. Excess stain was washed off, and the slides were air dried for 30 min. At least 100 metaphase spreads were scored from three independent experiments using Olympus BX53 microscope at 100X magnification.

QUANTIFICATION AND STATISTICAL ANALYSIS

Statistical significance for immunofluorescence and DNA fiber experiments was calculated using GraphPad Prism software (Version 6.0). For DNA fiber experiments, metaphase analysis, and immunofluorescence studies, Mann Whitney test was used. A one-way ANOVA test was used for SCR reporter-based FACS analysis and BrdU incorporation. The values of N and P are provided in each figure legend.